Capicua regulates neural stem cell proliferation and lineage specification through control of Ets factors

Shiekh Tanveer Ahmad[1,2,3], Alexandra D. Rogers[2], Myra J. Chen[2,3], Rajiv Dixit[2,3,4], Lata Adnani[3,4], Luke S. Frankiw[2,5], Samuel O. Lawn[2,6], Michael D. Blough[2], Mana Alshehri[2,7], Wei Wu[2,8], Stephen M. Robbins[2], J. Gregory Cairncross[2], Carol Schuurmans[3,4], Jennifer A. Chan[1,2,3,*]

[1] Department of Pathology & Laboratory Medicine, University of Calgary, Calgary, Alberta, Canada
[2] Charbonneau Cancer Institute, University of Calgary, Calgary, Alberta, Canada
[3] Alberta Children's Hospital Research Institute, University of Calgary, Calgary, Alberta, Canada
[4] Sunnybrook Research Institute and the Department of Biochemistry, University of Toronto, Toronto, Ontario, Canada

Present addresses:
[5] Department of Biology & Bioengineering, California Institute of Technology, Pasadena, CA, USA
[6] Zymeworks, Vancouver, BC, Canada
[7] King Abdullah International Medical Centre, Riyadh, Saudi Arabia
[8] University of California, San Francisco, CA, USA

*Corresponding author:
Jennifer A. Chan
University of Calgary
Heritage Medical Research Building, room 303
3330 Hospital Drive NW
Calgary, AB T2N 4N1
Canada
jawchan@ucalgary.ca

Keywords:
Capicua, CIC, oligodendroglioma, glioma, oligodendrocyte precursor cell, cell fate specification, gliogenesis, Etv5

ABSTRACT

Capicua (Cic) is a transcriptional repressor mutated in the brain cancer oligodendroglioma. Despite its cancer link, little is known of Cic's function in the brain. Here, we investigated the relationship between Cic expression and cell type specification in the brain. Cic is strongly expressed in astrocytic and neuronal lineage cells but is more weakly expressed in stem cells and oligodendroglial lineage cells. Using a new conditional *Cic* knockout mouse, we show that forebrain-specific *Cic* deletion increases proliferation and self-renewal of neural stem cells. Furthermore, *Cic* loss biases neural stem cells toward glial lineage selection, expanding the pool of oligodendrocyte precursor cells (OPCs). These proliferation and lineage selection effects in the developing brain are dependent on de-repression of Ets transcription factors. In patient-derived oligodendroglioma cells, CIC re-expression or ETV5 blockade decreases lineage bias, proliferation, self-renewal and tumorigenicity. Our results identify Cic is an important regulator of cell fate in neurodevelopment and oligodendroglioma, and suggest that its loss contributes to oligodendroglioma by promoting proliferation and an OPC-like identity via Ets overactivity.

INTRODUCTION

The identification of genes recurrently mutated in cancer often presents opportunities to uncover previously unappreciated mechanisms regulating normal development, and vice versa. The transcriptional repressor Capicua (*CIC*) has been identified as a likely tumour suppressor gene, as recurrent mutations in *CIC* and/or reduced expression of CIC are found in several cancer types. In the brain, *CIC* mutations are nearly exclusively found in oligodendrogliomas (ODGs) – glial tumors that are composed of cells resembling oligodendrocyte precursor cells (1, 2). Indeed, concurrent *IDH1/2* mutation, single-copy whole-arm losses of 1p and 19q, and mutation of the remaining copy of *CIC* on

59 chr 19q13 are highly characteristic of ODG and are not found in other cancer types (3-5). These
60 associations suggest a unique relationship between CIC and glial biology.
61
62 Prior work in Drosophila and in mammalian cultured cells has shown that Cic is a transcriptional
63 repressor downstream of receptor tyrosine kinase (RTK) signalling (6). Binding of Cic to the sequence
64 T(G/C)AATG(G/A)A in enhancers and promoters leads to transcriptional repression of its target genes
65 (7, 8). This default repression is relieved upon RTK signalling (6, 9-11), permitting transcription of
66 targets – among which are *PEA3/ETS* transcription factors *ETV1/4/5* (12). To date, there is limited
67 knowledge of Cic's function in mammalian development or in the brain. Recently, Yang et al. using *Cic*
68 conditional knockout mice, reported that Cic loss increases a population of proliferating Olig2+ cells in
69 the brain, and that) loss of Cic potentiates glial tumorigenesis in a glioma model driven by *PDGFR*
70 (13). The mechanisms by which Cic loss caused those findings, however, remained undefined.
71 Meanwhile, in the non-neoplastic context, Lu et al. recently showed that impairing the interaction of the
72 Cic with the protein Ataxin 1 results in spectrum of neurobehavioral and neurocognitive phenotypes,
73 as well as abnormal maturation and maintenance of populations of cortical neurons (14) – indicating a
74 role for Cic in neuronal biology as well. Deciphering Cic's mechanisms of action as a
75 neurodevelopmental regulator may shed light on these varied phenotypes resulting from Cic loss or
76 abnormal function.
77
78 Here, we examine the temporal and spatial pattern of Cic expression in the mammalian cerebral
79 cortex and white matter, and take a loss-of-function approach to determine its role in neuronal-glial
80 identity determination. Our results reveal an important role for Cic in regulating the proliferation and
81 lineage specification of neural stem cells during development – with loss favoring NSC proliferation
82 and glial production at the expense of neuronal production. Furthermore, we show that these effects
83 are mediated largely through Cic's regulation of Ets factors. The proliferative dysregulation is
84 recapitulated in oligodendroglioma cells, where CIC re-expression or blockade of Ets activity reduces

85 tumorigenicity. Our findings reveal an important role for CIC in development and oligodendroglioma,
86 and suggest that Etv5 may be a potential therapeutic target.
87
88 **RESULTS**
89
90 **Nuclear Cic levels are cell type- and stage-specific**
91
92 As an initial step to investigating Cic's potential function in forebrain development and
93 oligodendroglioma, we examined its expression in several regions and cell types in the mouse brain.
94 Immunofluorescence staining for CIC and cell-type specific markers revealed that all cell types
95 examined have some detectable level of Cic protein, whether cytoplasmic or nuclear. Because of Cic's
96 previously identified role as a transcriptional repressor, however, we were particularly interested in the
97 nuclear levels and quantitated Cic nuclear staining intensity across cell types and stages.
98
99 Focusing first on the stem cell compartment, we assessed tissue from the dorsal telencephalon (the
100 anlage of the neocortex) at embryonic day (E) E12. At this early neurogenic stage, non-lineage
101 restricted neural stem cells (NSCs) are found in the ventricular zone (VZ) where can be identified by
102 their spatial location and their expression of the transcription factor Sox2 (15). In embryonic Sox2+ VZ
103 cells, Cic was localized predominantly in the cytoplasm, with relatively weak nuclear expression
104 (Figure 1A). This distribution is consistent with the previous demonstration that growth factor/RTK
105 signaling is locally elevated in the embryonic VZ (16, 17) and that Cic nuclear export is regulated by
106 ERK-mediated Cic phosphorylation (6, 9-11). Pools of stem/progenitor cells are not limited to
107 development, but also persist postnatally in the subventricular zone (SVZ) of the lateral ventricle and
108 in the subgranular layer (SGL) of the hippocampal dentate gyrus (18, 19). In the SVZ and SGL of
109 postnatal day (P) P21 and P56 mice, Cic was also weakly expressed within the nucleus in the Sox2+
110 compartment – in contrast to stronger nuclear expression in adjacent differentiated cells (Figure 1B,C).

111 Thus, in both the embryonic and postnatal brain, neural stem cells are characterized by low levels of
112 nuclear Cic.
113
114 As cells differentiated, Cic was increasingly localized to the nucleus, but with notable differences
115 between the levels detected in neuronal, astrocytic, and oligodendrocytic cell lineages. In the adult
116 (P56) cortex, NeuN+ neurons displayed the strongest nuclear Cic (Figure 1I). The increase in Cic
117 within the neuronal lineage was detectable during the process of embryonic neurogenesis, with a
118 modest increase detected as cells transitioned from Sox2+ stem cells to Tbr2+ neuronal intermediate
119 progenitors, followed by a more marked elevation in Tbr1+ post-mitotic neurons in the intermediate
120 zone and cortical plate – where nuclear Cic levels approached those of mature neurons in the adult
121 cortex (Figure 1G,H,I, J). In GFAP+ or Aldh1+ astrocytes in the cortex and underlying white matter,
122 nuclear Cic levels also increased relative to Sox2+ cells (Figure 1D,J; Supplemental Figure S1A).
123 Among the three major lineages, the lowest levels of nuclear Cic were found in the oligodendroglial
124 lineage. Olig2 is a bHLH transcription factor that is expressed in cells at or before oligodendrocyte
125 specification and continues to be present throughout the stages of oligodendroglial differentiation (20,
126 21). Within the Olig2+ population, the subset of Pdgfra+ cells indicative of oligodendrocyte precursor
127 cells (OPCs) had the lowest levels of all, with a modest increase in CNPase+ immature
128 oligodendrocytes, and a further increase in mature CC1+ oligodendrocytes (Figure 1E, F, J; and Suppl
129 Fig S1). Overall, the mean integrated nuclear signal intensity for Cic was significantly lower in Sox2+
130 and Pdgfra+ cells than in NeuN+ cells ($p < 0.0001$), Tbr1+ cells ($p < 0.0001$), or Gfap+ cells ($p < 0.01$)
131 (Figure 1J and Suppl S1).
132
133 As both NSCs and OPCs are cell types that are proliferation-competent, this pattern of lower nuclear
134 Cic in NSCs and OPCs, and higher nuclear Cic expression in neurons and astrocytes, raised the
135 possibility that nuclear CIC bound to its target genes may repress proliferation-related genes and/or
136 early oligodendroglial-promoting programs. We tested these hypotheses with a series of loss-of-
137 function studies.

138

139 **Cic-deficiency results in increased glial populations and decreased neuronal populations**
140 **during forebrain development**

141

142 Cic contains several critical domains including an HMG-box and a C-terminal C1 domain that together
143 bind to DNA, and a C-terminal Gro-L domain that mediates protein-protein interactions (10, 22-25).
144 We generated *Cic* conditional knockout mice in which exons 2-11 of *Cic* gene were flanked by loxP
145 sites, with the floxed region containing all exons encoding the HMG box. Upon introduction of Cre,
146 exons 2-11 are excised and the remaining exons 12-20 are frameshifted, thus ablating the HMG box,
147 C1 domain, and Gro-L domain (Figure 2A). We used these animals for in vivo studies as well as to
148 generate cell lines with which we could further study proliferation and lineage selection in a cell-
149 autonomous manner.

150

151 By crossing *Cic*-floxed mice to *Foxg1-Cre* mice (in which *Cre* is expressed throughout the forebrain by
152 E10.5 (26)), we generated mice deficient in CIC in the embryonic telencephalon and subsequent
153 postnatal cerebrum (Figure 2A,B). $Cic^{Fl/Fl};FoxG1^{Cre/+}$ animals were born in approximate Mendelian
154 ratios and were grossly indistinguishable at birth. They failed to thrive postnatally, however, becoming
155 visible runts by postnatal day 7, and were uniformly lethal by P22 when they did not survive past
156 weaning. The reason for lethality is unclear. Gross and cursory light microscopic exam showed the
157 presence of the expected major anatomic structures in the brain, as well as the presence of laminated
158 cortex, white matter tracts, deep nuclei, and hippocampi. The cerebra of Cic-null brains, however,
159 were smaller than littermate controls (Figure 2C, Suppl Fig 2). We have not found major anatomic
160 defects in other organs and suspect that poor feeding secondary to impaired neurologic function may
161 be related to their progressive decline.

162

163 Microscopic exam showed that the overall decrease in cerebral size in CIC forebrain-null animals was
164 due to global decreases in volume that affected both gray matter and white matter structures (Suppl

165 Fig S2A-C). The corpus callosum of null animals was thinned but showed abnormally increased
166 cellularity (Suppl Fig S2B). The cortex was also thinner in Cic-null brains, again showed increased
167 cellularity (Suppl Fig S2C,D). Interestingly, cortical neuronal density was not significantly different
168 between the two (Suppl Fig S2E), suggesting that the increased cellularity in the mutant brains could
169 be due to increased glia, and also that the total number of cortical neurons was decreased (same
170 neuronal density, but an overall smaller cortical volume).
171
172 Closer evaluation of P21 cortices confirmed this shift in cell populations, with decreased neurons and
173 increased oligodendroglia cells and astrocytes in Cic-null cortices and white matter compared to
174 controls (Fig 2D,D',E,E'). In Cic-null cortices, NeuN+ cells comprised 76.6±2.5% of total cells; whereas
175 in controls that were either CIC-floxed but without Cre ($Cic^{Fl/Fl}$; $FoxG1^{+/+}$) or that were heterozygous for
176 Cic loss ($Cic^{Fl/+}$; $FoxG1^{Cre/+}$), NeuN+ cells comprised 82.04±2.78% of the total cells (n=5, $p<0.05$). In
177 contrast, Gfap+ cells were increased in knockout relative to wild-type cortices (12.46±1.49 CIC-null *vs.*
178 9.61±1.39 Cic-wt; 1.29-fold change; n=5, $p<0.05$). Olig2+ cells were also increased in Cic-null cortices
179 compared to controls (10.83±1.47% *vs.* 4.99±0.87%, in Cic-null vs control, respectively; 2.17-fold
180 increased; n=5, p=0.0001), a finding corroborated by an increase in Sox10+ cells (11.72±1.83% *vs.*
181 7.43±0.94%; n=5, p=0.0001). In the progression along the oligodendrocyte lineage, the relative
182 distribution of cells was also altered. Olig2+Sox2+ cells were increased in Cic-null animals
183 ($CIC^{Fl/Fl}$;$FoxG1^{Cre/+}$ 13.67±2.89% vs. Control 4.31±1.33%; n=3, $p<0.01$)(Suppl Fig S3) as were
184 Olig2+Pdgfra+ OPCs (44.53±3.80% of cells Olig2+Pdgfra+ in $CIC^{Fl/Fl}$;$FoxG1^{Cre/+}$ *vs.* 28.20±1.95% in
185 controls; $p<0.01$). In contrast, CNPase+ cells were comparatively decreased ($CIC^{Fl/Fl}$;$FoxG1^{Cre/+}$
186 38.0±9.78% *vs.* Control 72.92±3.88%; n=5, $p<0.0001$) (Figure 2E,E'). Mbp expression in the white
187 matter was also decreased in $Cic^{Fl/Fl}$;$FoxG1^{Cre/+}$ brains (n=6, $p < 0.01$) (Figure 2E,E').
188
189 One possibility that could explain such a skewing of cell populations could be that there was increased
190 death in a particular population. However we found no evidence of increased apoptosis in the
191 knockout brains (Suppl Fig S4E). Other possibilities, were that Cic loss could be increasing

192 proliferation and affecting lineage selection in NSCs, or that Cic loss could have specific effects on
193 OPC proliferation and maturation – possibilities that are not mutually exclusive. In the following work,
194 we focus our investigations on Cic's role at the NSC stage, and examine its role in proliferation and
195 lineage selection.
196
197 **CIC increases proliferation of neural stem cells**
198
199 Others recently reported proliferative gains upon loss of Cic (13), and we too found evidence of this.
200 By electroporating pCIG2-Cre (or pCIG2 empty vector control) into *Cic*$^{Fl/Fl}$ embryos, we could study the
201 effects of Cic loss in a discrete population of VZ cells and their subsequent progeny (schematic Figure
202 4A). 48 hours after Cre electroporation into VZ NSCs at E13 (early to mid-neurogenesis), EdU
203 incorporation was markedly increased, as were the numbers of Sox2 positive cells. Among GFP+
204 cells, EdU+ cells were increased by 2.6-fold in cre- vs. control-electroporated brains (pCIG2-Cre
205 9.99±0.92% Edu+, n=4, *vs.* pCIG2-Empty; 3.77±0.81%, n=5, $p<0.0001$)(Figure 3A,A'). The fraction of
206 GFP+ cells expressing Sox2 was also increased (pCIG2-Cre 11.09±1.10% Sox2+ vs. pCIG2-Empty
207 5.48±1.01%; n=4 and n=5, respectively; $p<0.05$) (Figure 4B,B'). There was no change in activated
208 Caspase-3, indicating that the increased Sox2+ fraction in Cic-deleted cells was not due to increased
209 apoptosis in other cells (Suppl Figure S4D,D'). Together, these findings supported a cell-autonomous
210 increase in NSC proliferation with CIC loss. Of note, there was also an increase in Edu+ cells among
211 non-GFP cells within the area of the electroporated patches, suggesting additional non-cell
212 autonomous effects that we did not pursue.
213
214 To confirm the cell autonomous gains in NSC proliferation with CIC ablation, we turned to cell culture.
215 *Cic* null and control NSC lines were derived from E15 *Cic*-floxed cells transfected ex-vivo with Cre or
216 control plasmids (Figure 3B). When maintained in serum-free NSC proliferation media, Cic-null and
217 control cells both maintained expression of NSC markers such as the intermediate filament protein
218 nestin (Figure 5A,B). When Cic-null and control cells were seeded at equal numbers and grown in

219 NSC proliferation media, however, Cic-null cells displayed a 3-fold increase in cell numbers relative to
220 controls by 3 days post-plating (Cic-null; 2.90±0.44, n=4, *vs.* Cic-wt; 0.98±0.12, n=3, $p<0.01$) (Figure
221 3C). These data were corroborated by Alamar blue cell viability assay (Suppl Figure S4A), Ki-67
222 immunostaining (Figure 3D) and cell cycle analysis (Figure 3E), all of which showed increased
223 proliferation in Cic-null cultures compared to controls. There were no significant differences in the
224 numbers of dead cells (Suppl Figure S4C), supporting that the differences in viable cell numbers for
225 Cic-null cells was due to their higher proliferative rates, rather than reduced cell death. Together, the
226 data show that Cic is a strong negative regulator of proliferation in forebrain NSCs.
227
228 ***Cic* loss alters mode of cell division and self-renewal**
229
230 During mammalian neurodevelopment, the stem cell pool is first expanded by symmetric proliferative
231 cell divisions followed by rounds of asymmetric divisions of stem and progenitor cells, which generate
232 neurons and then glia, and finally by terminal symmetric differentiative divisions (18). The balance
233 between symmetric and asymmetric divisions is important for maintaining the stem/progenitor pool,
234 and alterations in cell division mode can lead to neoplasia (27).
235
236 To investigate whether *Cic* loss alters modes of cell division, we performed a paired cell assay. *Cic*
237 null and control NSCs were seeded at low density in adherent cultures for 24 hrs, then fixed and
238 stained for Ki-67 (Figure 3G). Pairs where both daughter cells were Ki67+ were scored as symmetric
239 proliferative divisions. Pairs where daughter cells differed in Ki67 expression (i.e. Ki67+/Ki67-) were
240 scored as asymmetric. Pairs where both daughter cells were Ki67- were scored as symmetric
241 terminal. *Cic* null cells underwent significantly more frequent symmetric proliferative divisions (77.6 ±
242 10.2% vs. 24.3 ± 4.9%; $p < 0.01$, n=3) and fewer asymmetric divisions (9.7 ± 1.2% vs. 64.0 ± 7.1%; p
243 < 0.05, n=3) compared to controls (Figure 3H). No significant difference was found in numbers of
244 symmetric terminal divisions between *Cic* null and control cells, although there was a trend toward

245 decreased terminal divisions in CIC null cells (12.7 ± 8.1% vs. 25.0 ± 6.5%; n=3, p = 0.108)(Figure
246 3H). The net effect of these is the presence of more cycling and self-renewing cells.
247
248 Consistent with this, evidence for increased self-renewal in the Cic null cells was also detected in a
249 clonogenic assay (Figure 3F). In this assay, after plating equal numbers of dissociated cells in semi-
250 solid media, a higher number of spheres indicates higher number of self-renewing cells in the initial
251 population, whereas sphere volume is a more general indicator of proliferation that includes the
252 influence of factors such as cell cycle kinetics, modes of cell division, and the fraction of cells
253 remaining in or exiting the cell cycle. Both Cic-null and control NSCs were able to generate spheres,
254 but Cic-null NSCs NSCs generated higher sphere counts (n=3; p < 0.0001) and larger spheres
255 compared to control (n=3; p<0.0001)(Figure 3F,F',F''). Thus, Cic loss confers not only higher
256 proliferation but higher self-renewal capacity in NSCs, at least when cells are in an environment
257 promoting NSC proliferation.
258
259 ***Cic* ablation in NSCs increases the pool of cells expressing glial lineage determinants**
260
261 While the proliferative effects of Cic deficiency in NSCs were clear, what was intriguing was the
262 additional possibility that Cic loss may be affecting lineage selection in NSCs. As the $Cic^{Fl/Fl};FoxG1^{Cre/+}$
263 phenotype was characterized by a shift in cell populations with fewer neurons and increased glia
264 (Figure 2), we thus asked whether Cic loss had altered the expression of factors important in
265 regulating lineage selection and gliogenic potential.
266
267 To this end, we examined the expression of Sox 9 and Olig2 in Cic-wildtype and -null NSCs. Sox9 is
268 an HMG-box transcription factor present in a range of CNS cell types, including stem cells, astrocyte
269 and oligodendroglial precursors, and later glial cells. It has key roles not only in stem cell maintenance
270 but also in driving differentiation programs away from neurogenesis and towards gliogenesis of both
271 astrocytes and oligodendrocytes at the stage of gliogenic initiation (28-30). Similarly, Olig2 is

272 expressed in a multitude of cells including stem cells, oligodendroglial lineage cells, and specific
273 subtypes of neurons; but it has a major role in establishing oligodendroglial competence. In our
274 control or cre-electroporated brains where Cre was introduced at E13, we found that the fraction of
275 GFP+ cells expressing Sox9 was 2.5-fold increased over controls at 2 days post-electroporation
276 (pCIG2-Cre; 15.97±1.69% *vs.* pCIG2-Empty; 6.37±1.60%, n=4 $p<0.05$) (Figure 4C,C'). Following the
277 targeted cells to E18 (5 days post-electroporation) revealed that a smaller fraction Cic-deleted NSCs
278 subsequently became Tbr1+ early-born/deep-layer neurons (pCIG2-Cre 1.66±0.91% *vs.* pCIG2-Empty
279 4.62±1.04%; n=5, $p<0.01$) (Figure 4D,D'). Conversely, a greater number fraction became Aldh1+
280 astrocytes (pCIG2-Cre 3.65±1.31%, n=5, *vs.* p-CIG2-Empty 1.664±0.91%, n=6; $p<0.05$) or Pdgfra+
281 OPCs (pCIG2-Cre 13.29±1.04%, *vs.* p-CIG2-Empty 5.87±2.54%; n=4; $p<0.01$) (Figure 4C,C',E,E').
282
283 These findings were echoed in the expression of stem and lineage markers in the cultured NSCs. As
284 expected, when cells were grown in NSC media, both Cic-null and control cells both strongly
285 expressed Nestin, and were largely devoid of Gfap or the pan-neuronal marker βIII-Tubulin (as
286 detected by Tuj1)(Figure 5A,B), or markers of subsequent oligodendrocyte stages, including OPCs,
287 mature, and myelinating oligodendrocytes (not shown). There, was, however, a marked increase in
288 the percentage of cells expressing Sox9 and Olig2 in Cic-null cultures (Figure 5A,A'). Sox9+ cells
289 were increased 3.04-fold in Cic-null cultures compared to control (Cic-null 37.4±3.6% *vs.* Cic-wt
290 12.3±2.1%; n=3, $p < 0.01$)(Figure 5A,B) while Olig2+ cells were increased 2.09-fold (Cic-null
291 29.8±2.9% *vs.* Cic-wt 14.2±3.5% in controls; n=3, $p<0.01$) (Figure 5A,A'). Western blotting also
292 corroborated the findings (Figure 5B). A possible interpretation of the increased Sox9 and Olig2
293 concurrent with Nestin positivity in Cic-null cells is that Cic loss may set an intrinsic foundation for pro-
294 glial or pro-oligodendroglial programs starting early in the neural cellular hierarchy.
295
296 **Cic-deficient NSCs are less responsive to extrinsic neuronal and astrocytic lineage selection**
297 **cues, but are biased to oligodendroglial lineage selection**
298

299 To directly test cell type specification capacity, we challenged Cic-null and control NSCs with exposure
300 to different lineage-promoting culture conditions. Neuronal differentiation was induced by culturing
301 cells with B27 and cAMP. Astrocytic differentiation was induced by culturing NSCs in 1% FBS and N2.
302 Oligodendroglial differentiation was induced by culturing cells in media with B27 and tri-iodo-thyronine.
303 After a 10 day exposure to these conditions, cultures were analyzed for cellular identity and
304 morphology.
305
306 After 10 days in the neuronal condition, fewer Tuj1+ cells were generated in absolute numbers in Cic
307 null cultures compared to controls after plating equal numbers of starting cells (1.967±0.36 $x10^3$ vs
308 2.929±0.33 $x10^3$ Tuj1+ per well in Cic-null vs control; $p<0.05$)(Fig 6G) – a finding corroborated by
309 western blotting for Tuj1 (Figure 5C'). Furthermore, of the cells that were Tuj1+, we observed fewer
310 and less complex cell processes in the Cic-null cells than in their Cic-wildtype counterparts (Figure
311 5C). In the astrocytic condition, there were fewer absolute numbers of Gfap+ cells in the Cic-null
312 cultures (1.471±0.15 $x10^3$ vs 2.74±0.55 $x10^3$ Gfap+ per well in Cic-null vs control, $p<0.05$) (Fig 6F).
313 Western blotting also showed decreased GFAP (Figure 5D'). Analogous to our observation in the
314 neuronal differentiation condition, Gfap+ Cic-null cells in the astrocytic differentiation condition
315 displayed more rudimentary processes than their Cic-wildtype counterparts (Figure 5D). In both of
316 these conditions, there were only a few proliferating cells remaining after the differentiation protocols,
317 consistent with successful differentiation. In both conditions, there was also no change in apoptotic
318 cells (Suppl Figure S4F-F'''). When viewed as fractions of the total cell population, Cic-null cultures
319 were comprised of a significantly smaller fraction of bIII-Tub+ (Tuj1+) neurons in the neuronal
320 condition (CIC-null 24.0±9.2% *vs.* CIC-wt 67.8±8.5%, respectively; n=3, $p<0.01$) and a significantly
321 smaller fraction of Gfap+ cells in the astrocytic condition (29.1±5.5% in Cic-null *vs.* 68.2±10.4% in Cic-
322 wt; n=3, $p <0.01$)(Figure 5C,D). Thus, with normal CIC expression, NSCs that are exposed to neuronal
323 conditions become neurons (as expected), but CIC-deficient NSCs do not as readily select the
324 neuronal lineage when exposed to the same neuronal-inducing conditions. Likewise, most CIC-wt
325 NSCs that are exposed to astrocytic conditions become astrocytes (as expected), but CIC-null NSCs

326 do not as readily select the astrocytic lineage when exposed to the same astrocyte-inducing
327 conditions. Together, the data indicate that Cic-deficient NSCs are less responsive to external cues
328 for neuronal and astrocytic lineage specification.
329
330 We then asked what the Cic-null NSCs became, if not neurons and astrocytes, respectively. In the
331 neuronal condition, the Tuj1- population was predominantly comprised of Sox2+ cells, followed by
332 Olig2+ cells; together, half of the culture was comprised of either Sox2+ (31%) or Olig2+ cells (19%)
333 after exposure to the neuronal conditions (Figure 6B',B'''). Of the Sox2+ and Olig2+ cells present,
334 however, less than 1% were EdU+, and there was no significant difference between the proliferation
335 rate of Sox2+ or Olig2+ cells in the Cic-null vs. control cultures in the neuronal condition (Figure 6D-
336 E). There was also a small but non-significant increase in the percentage of Gfap+ cells in the Cic-null
337 cultures compared to control. In the astrocytic culture condition, the Gfap- population was also
338 comprised predominantly of Sox2+ cells and, to a lesser extent Olig2+ cells, both of which were
339 significantly increased in the Cic-null cultures compared to controls. 36% of the Cic-null cells in the
340 astrocytic condition still expressed Sox2 after the 10-day protocol (Figure 6A'''). Tuj1+ cells were rare
341 in the astrocytic condition in both Cic-null and control cultures. These data further support that CIC-
342 deficient NSCs are less responsive to neuronal and astrocytic lineage cues, and instead remain as
343 stem cells that are permissive to the oligodendroglial lineage.
344
345 After 10 days in the oligodendrocyte-promoting media both Cic-null and wildtype cultures contained a
346 mix neurons, astrocytes, and oligodendrocytes; however the distributions of cells between cell types
347 and also along stages of oligodendrocyte lineage progression were altered. There was a higher
348 fraction of Olig2+ cells in Cic-null cultures compared to control (Cic-null 68.0±1.6% *vs.* Cic-wt
349 54.1±0.9%; n=3, $p < 0.01$) as well as increased Olig2 by western blotting (Figure 5E). When analyzed
350 for markers of OPCs versus more mature oligodendroglial markers, Cic-null cells also had a greater
351 percentage of Olig2+ Pdgfra+ cells than in Cic-wildtype cultures (Cic-null 68.8±2.4% vs. Cic-wt
352 39.3±3.8%; n=5, $p < 0.0001$)(Figure 5E). Conversely the percentage of Olig2+MBP+ cells was

353 decreased in Cic-null cultures compared to controls (Cic-null 2.1±1.5% vs. Cic-wt 8.2±3.0%; n=5, $p < 0.0001$)(Figure 5E). Of the few Cic-null Olig2+MBP+ cells that were identified, process formation was rudimentary compared to Cic-wildtype cells. With respect to other cell types present in the oligodendroglial culture conditions, Sox2+ cells were increased in Cic-null cultures compared to control, whereas both Tuj1+ and Gfap+ cells were reduced (Figure 6C-C'''). 358

359 The results suggest to us that Cic-null cells are less sensitive to neuronal or astrocytic differentiation signals but retain permissiveness to the oligodendroglial lineage. Cumulatively, based on the pattern of cell-type specific nuclear Cic expression in forebrain tissue together with the in vivo and in vitro functional studies of Cic ablation, we conclude that Cic is a critical regulator of proliferation, self-renewal, and cell fate of NSCs. Loss of Cic expands the OPC pool by not only increasing NSC proliferation but also biasing their specification towards the oligodendroglial lineage. 365

366 **Ets factors are transcriptional repressive targets of Cic in the forebrain** 367

368 As Cic is a transcriptional repressor, one mechanism for our findings is that Cic loss de-represses specific genes driving NSC proliferation and lineage specification. In this respect, *Etv* genes, which encode Ets-domain transcription factors, are candidate target genes of interest. *Etv* genes (Etv 1, 4, 5) have been identified as direct targets of Cic in various mammalian cells and tissues (12, 31), and are overexpressed in ODGs (32). Furthermore, previous studies have documented Cic occupancy at the *Etv5* promoter, at least in cerebellar tissue (33). Consistent with a possible functional relationship between CIC and Ets factor gene regulation in the forebrain, we found that NSCs and OPCs, the two cell types that have the lowest levels of nuclear Cic, express the highest levels of Etv4 and 5 (Figure 7F-K; Supplemental Figure S5B-D'). We also confirmed that in forebrain tissue, *Etv5* showed evidence of promoter occupancy by Cic via ChIP-PCR (Figure 7C). 378

379 If Ets factors are the mediators of the effects of CIC loss that we observe, we would expect their levels
380 to be elevated in our experimental systems of CIC loss. Indeed, we found that *Etv4* and *Etv5*
381 transcript levels were elevated in cultured Cic-null cells compared to control cells after 2 days of
382 growth in oligodendroglial conditions. *Etv5* mRNA was increased ~37 fold while *Etv4* transcripts were
383 increased ~19 fold in Cic-null cells versus control cells whereas *Etv1* transcripts were unchanged
384 (Figure 7A). Western blotting also confirmed marked increases in levels of Etv4 and Etv5 in Cic-null
385 cells (Figure 7B). Although both *Etv4* and *Etv5* were both de-repressed upon Cic loss, because of the
386 comparatively higher levels of Etv5 relative to Etv4, as well as previous studies implicating *Etv5* in
387 mediating glial fate decisions (34), we focused additional studies on this Ets factor. In vivo
388 electroporation of *Cic* shRNA into the telencephalic VZ resulted in upregulation of *Etv5* transcript in the
389 electroporated patch within 48 hours (Figure 7D). Our *Cic*-floxed, Cre-electroporated brains showed a
390 similar increase in Etv5 protein in the electroporated patch (Figure 7E). In aggregate, these data
391 support that the PEA3 Ets transcription factors are transcriptional repressive targets of Cic in the
392 forebrain.
393
394 **Ets de-repression mediates the proliferative and oligo-biased phenotype of *Cic*-deficient NSCs**
395
396 To determine whether the increased proliferation and OPC bias that we observed with CIC ablation
397 was mediated by Etv5, we overexpressed wild-type *Etv5*. In vivo, electroporation of wild-type *Etv5*
398 phenocopied the increase proliferation of CIC-null cells in vivo (Figure 8D, D', S6A). Similarly, *Etv5*
399 overexpression acutely increased proliferation of cultured NSCs (Figure 8F, S6C'). We also performed
400 epistasis experiments introducing a dominant negative form (*DNETV5*) in which *Etv5* was fused to the
401 *Engrailed* transcriptional repressor domain. Introduction of *DNETV5* or knockdown of *Etv5* with siRNA
402 reduced the proliferation of cultured *Cic*-deficient NSCs back to control levels (Figure 8F-G, Suppl
403 Figure S6D). In vivo, the increased proliferation observed upon deletion of *Cic* by cre-electroporation
404 was abrogated by co-electroporation with *DNETV5,* resulting in proliferation that was comparable to
405 baseline (Figure 8E, E' compared to 8D,D'; Figure S6). Based on the extent of the effects of *Etv5*

406 overexpression and *DNETV5* rescue in these assays, we conclude that the proliferative effects of Cic
407 loss are large driven by de-repression of Etv5.
408
409 With respect to the altered proportions of cell types that we had observed in CIC-deficient NSCs
410 exposed to the different lineage-specific culture conditions, overexpression of wild-type Etv5 also
411 phenocopied CIC loss in many respects. There were decreased fractions of Tuj1+ cells and Gfap+
412 cells in the neuronal and astrocytic conditions, and increased fractions of Olig2+ and Olig2+Pdgfra+
413 cells in the oligodendrocytic condition when Etv5 was overexpressed – although the severity of the
414 changes was somewhat less marked with Etv5 overexpression compared to Cic loss. DNETV5 was
415 also able to substantially (although incompletely) rescue the phenotype of Cic-deficient cells in these
416 assays. In the neuronal and astrocytic conditions, DNETV5 significantly increased the populations of
417 Tuj1+ and Gfap+ cells, respectively. The shifts in Olig2+ cells and Olig2+Pdgfra+ OPCs returned to
418 control levels (44.6±12.0% in *Cic*^{null}*;DNETV5* cells *vs.* 62.5±14.6% in *Cic*^{null} cells; n=3, $p<0.05$). The
419 percentage of cells expressing MBP also showed a substantial although partial rescue (5.3±2.9% in
420 *Cic*^{null}*;DNETV5* cells *vs.* 2.1±1.5% in *Cic*^{null} cells; n=3, $p < 0.05$) (Figure 8C-C'). That the extent of the
421 changes for the lineage selection assays with Etv5 overexpression and DNETV5 rescue were partial
422 suggests that other factors may contribute to the lineage specification affects, nevertheless the results
423 point to Etv5 as playing a large part in the lineage phenotype.
424
425 Thus, Etv5 is both necessary and sufficient for inducing the proliferation and cell fate bias effects
426 downstream of CIC loss.
427
428 **Ets blockade decreases proliferation, self-renewal, and tumorigenicity of human**
429 **oligodendroglioma cells**
430
431 Finally, we used 2 oligodendroglioma cell lines, BT54 and BT88, to further investigate the importance
432 of *CIC* mutation/loss in human disease. Both of these patient-derived lines harbour the characteristic

433 whole-arm chromosome 1p and 19q losses that are diagnostic of ODG (35). As well, BT54 harbours a
434 splice acceptor site mutation in the remaining *CIC* exon 6 while BT88 harbours a missense mutation in
435 the remaining *CIC* exon 20 (3). In both BT54 and BT88, either stable re-expression of wildtype CIC or
436 stable expression of *DNETV5* significantly reduced proliferation as measured by EdU incorporation
437 (Figure 9A,A',C). Sphere-forming ability was also decreased by *CIC* expression or by introduction of
438 *DNETV5* (Figure 9B,B',B'',D,E). These results were also confirmed by transient siRNA experiments to
439 knock down Etv5 in BT-88 cells that also showed decreased proliferation and sphere formation (data
440 not shown). Consistent with an ongoing requirement for CIC loss or Etv5 expression for proliferation
441 and self-renewal in ODG, in vivo tumorigenicity of BT88 cells was markedly reduced, and survival of
442 animals was increased, by stable expression of either wildtype *CIC* or *DNETV5* (Figure 10). Thus, in
443 cells that are already transformed to ODG, CIC loss and the subsequent elevation of Etv5 remains
444 important to sustain the proliferative phenotype.
445
446 A similar finding was observed when we assessed the ODG cell lines' ability to differentiate in
447 response to oligodendrocyte differentiation conditions. Both CIC re-expression and DNETV5 similarly
448 resulted in increased expression of CNPase in the ODG cells compared to respective control cells,
449 indicating at least some improvement in capacity for the tumour cells to differentiate and mature
450 (Figure 9F,F' bottom row panels; Suppl Fig S7). Interestingly, however, effects on neuronal and
451 astrocytic differentiation, were mixed (Figure 9F,F' top and middle row panels). Cic re-expression
452 resulted increased the ability of cells to respond to extrinsic neuronal differentiation cues by increasing
453 expressing bIII-Tubulin (TUJ1) and extending neurites; however this was not phenocopied by
454 DNETV5. With respect to expression of GFAP in response to astrocytic differentiation cues, no
455 significant differences were detected with either CIC re-expression or DNETV5 introduction compared
456 to BT-88 control. The latter data suggest that other genetic (or epigenetic) alterations may be more
457 central to driving or maintaining some specific aspects of the tumour cells' phenotypes, at least in our
458 cultured system. The effects on differentiation in vivo were not evaluated, however, as the lesions

459 resulting from implantation of CIC- or DNETV5-expressing BT88 cells were too small to provide
460 meaningful cell numbers for assessment.
461
462 Taken together, our results indicate that Cic regulates NSC proliferation and cell fate in
463 neurodevelopment and oligodendroglioma, and that the pro-proliferative and pro-OPC phenotypes
464 observed with Cic loss are largely mediated through Ets transcriptional de-repression.
465
466 **DISCUSSION**
467
468 Genomic analyses of brain cancers have suggested that *CIC* functions as a tumor suppressor gene in
469 diffuse gliomas, particularly ODGs (3, 4, 36). Yet, to date, knowledge of *CIC*'s role in the brain has
470 been limited. Here we report previously undescribed cell type specific differences in CIC expression in
471 the brain. Moreover, our functional work examining *Cic* function in forebrain development and in
472 oligodendroglioma cells provides new insight into the roles of this putative tumor suppressor in
473 regulating the developmental fate of neural stem/progenitor cells.
474
475 We found that genetic ablation of Cic biases cells neural stem cells away from neuronal lineage
476 specification to the selection of glial lineages. Adding to knowledge that RAS/MAPK pathway
477 signaling regulates the switch from neurogenesis to gliogenesis, with *ETV5* implicated in mediating
478 gliogenic competence (17, 34), our results firmly place *Cic* at the intersection of RAS pathway
479 signaling and *Etv5* in the brain, providing a missing link between extrinsic differentiation signals and
480 the execution of transcriptional programs critical for normal neuro- and glio-genesis. With respect to
481 Cic and the anti-neuronal bias that we observed, recent work by Lu, et al. found that disrupting Ataxin-
482 1 (Atxn1)-Cic complexes resulted in abnormal maturation and maintenance of upper-layer cortical
483 neurons – with concomitant effect on behavior, learning, and memory (14). It is unknown, however,
484 the extent to which the effects could be due to specific Ataxin-Cic interactions versus Cic abnormality
485 alone. Our studies, which primarily focused on early lineage selection events, did not systematically

486 address questions of cell maturation (although some of our in vitro morphological findings are
487 consistent with a neuronal maturation defect). Future work would be needed to define the complex
488 neuronal dependencies on Cic, not only in the forebrain but also in the cerebellum where Cic
489 pathology has also been implicated (37) (38).
490
491 With respect to neural stem cell proliferation, glial fates, and the implications for ODG; our findings
492 build on the recent observation by Yang, et al. that CIC deficiency increases a population of
493 proliferating OPCs in the brain (13). Our work is not only consistent, but now provides a mechanistic
494 foundation for the observations with identification of symmetric cell division alterations, dissection of
495 lineage selection effects and identification of a downstream mediator. Together, they provide tangible
496 links between *CIC* loss and ODG biology – as both dysregulated proliferation and the persistence of
497 an immature OPC phenotype are cardinal features of this cancer. Many parallels exist between normal
498 OPCs and the cells comprising ODG. In common, both OPCs and ODGs express PDGF, PDGFR,
499 and NG2, which control OPC differentiation (39, 40). Together, the results may thus explain some of
500 these phenotypic features of ODG, and consistent with other reports suggesting that dysregulation of
501 OPCs or OPC-like cells are amongst the early changes in experimental models of gliomagenesis (2,
502 41).
503
504 There are some notable differences between the work reported by Yang, et al. (13), however, and our
505 studies. One difference is that the prior study used HOG cells that, despite their historic name, do not
506 carry the ODG-defining genetic features of 1p19q loss or *CIC* mutation; similarly the Pdgfra-
507 amplified/overexpressed mouse glioma model used is more akin to an RTK-driven GBM than it is to
508 ODG. In deploying the BT-88 and BT-54 models (which genetically and phenotypically faithfully
509 recapitulate ODG), our work may be closer to clinical relevance for ODG. Another difference is that
510 our studies also further clarify the early neuronal-glial fate decision effects of NSCs, with the bias away
511 from neuronal fates and toward glial fates in the setting of CIC loss. Most importantly, however, we

512 now identify *Ets* de-repression as a key mechanism underlying much of the phenotypic effects of Cic
513 loss in NSCs.
514
515 Our observation that *DN-Etv5* alone can abrogate so much of the pro-proliferative and pro-OPC
516 phenotype resulting from *Cic* loss was somewhat unexpected. In support of a role specifically for Etv5,
517 our observation that it is the most upregulated factor upon Cic loss, our Etv5 overexpression studies
518 (in vivo and in vitro), and our in vitro Etv5 siRNA experiments all lend independent support pointing to
519 the requirement for this particular Ets factor. However, we do not exclude that other Ets factors such
520 as Etv4 may also contribute. The dominant negative construct may not be entirely specific for
521 inhibiting Etv5 alone; such cross-reactivity has been reported with similar approaches, and further
522 experiments would be required to dissect the relative contribution of different Pea3 factors or other
523 subfamilies of the Ets genes. Nevertheless, the identification of this family of genes as a likely
524 mediator is salient to the development of future therapeutic strategies for ODG. Although it is thought
525 that transcription factors are difficult to target, reports of inhibition of other Ets factors either through
526 peptidomimetic or small molecule approaches (42-44) lend hope that Etv5 could potentially be
527 inhibited for clinical benefit.
528
529 Finally, although our findings are relevant to ODG biology, it is recognized that our studies do not
530 directly model the genesis of ODG. Indeed, despite the increase in proliferation observed in Cic-null
531 cells, no tumors were detected when following for up to one year after *Cre* electroporation of the *Cic*
532 floxed mice (data not shown) – in keeping with the concept that several collaborating genetic hits are
533 necessary for oncogenic transformation. Our *Cic* conditional knockout mice, however, will be a useful
534 tool for a future more refined cell type- and stage-specific deletion of *Cic* along with the introduction of
535 other mutations such as of *IDH1*(R132H) (45). We conceptualize *IDH1/2* mutations as a first event in
536 ODG, causing epigenetic changes that that serve to expand the potential pool of cells vulnerable to
537 transformation, with second-hit loss of *CIC* serving to dysregulate proliferation, bias cells to
538 oligodendroglial lineage, and delay them in an immature state. Additional studies using experimental

539 models and human ODG samples are needed to further dissect the relationship of *CIC* mutation to
540 *IDH* mutation. Although one recent study used single-cell RNA-Seq to examine ODG cell
541 subpopulations and did not detect any differences between ODG cells with and without *CIC* mutation
542 aside from the increased expression of PEA3 Ets factors, the number of cells analyzed was limiting for
543 resolution of cell type specific differences, and functional studies had not been performed (46). Similar
544 approaches with larger cell numbers might provide further insight into the biology of ODG with respect
545 to *CIC*.
546
547 In summary, we provide evidence that Cic regulates proliferation, fate decisions, and differentiation in
548 neural stem cells, with loss particularly expanding the OPC population. Furthermore, our findings
549 indicate that disruption of the Cic-Etv axis (with abnormal de-repression of *Etv5* downstream of *Cic*
550 loss) is central to the biology of ODG.
551
552

553 **METHODS**

554

555 **Mice**

556

557 CD1 outbred mice (Jackson Labs) were used for Cic expression analyses.

558

559 *Cic* conditional knockout (*Cic*-CKO) mice were generated at Taconic Artemis by homologous
560 recombination to flank Cic exons 2-11 with loxP sites. The exons targeted are 2-11 of *Cic* short form,
561 transcript variant 1, NM_027882.4 (equivalent to exons 3-12 of the *Cic* long form, NM_001302811.1,
562 Cic transcript variant 4). The targeting vector was generated using clones from the C57BL/6J RPCIB-
563 731 BAC library, and consisted of a 4.0 kb 5' flanking arm, neomycin resistance cassette (flanked by
564 FRT sites), 5.5 kb loxP-flanked region, a puromycin resistance cassette (flanked by F3 sites), and 6.0
565 kb 3' flanking arm. After homologous recombination in C57BL/6N Tac ES cells, generation of chimeric
566 animals, and germline transmission, Neo^R and $Puro^R$ cassettes were removed via Flp recombination
567 by breeding with a Flp deleter line. The
568 final CIC-CKO allele carries loxP sites in introns 1 and 11, and single residual FRT and F3 sites.
569 Expression of Cre recombinase results in deletion of exons 2-11 and frameshifting of the remaining
570 CIC-S exons 12-20. Genotyping primers were as follows: CIC 5' flanking region (192 bp wt, 348 bp
571 CKO allele) 5'- AGG AGG TTG TTA CTC GCT ATG G -3' (forward) and 5'- CTG ATG TCC TAA GAC
572 CTT TAC AAG G -3' (reverse); CIC 3' flanking region (273 bp wt, 410 bp CKO) 5' – CTG TGT CAC
573 TGT CTG CCT TCC -3' (forward) and 5' – TGG GTA ATA CCA CCG TGC C – 3 (reverse)'.

574

575 *FoxG1-cre* mice (Jackson Labs) were bred to *Cic*-CKO mice to generate telencephalic CIC knockouts
576 and littermate controls. After euthanasia, dissected brains were processed for histology, western
577 blotting, or cell culture. Knockout in tissue or cells post-cre was confirmed by Q-RT-PCR using
578 primer/probe sets for CIC (Applied Biosystems) and by Western blotting with anti-Cic.

579

580 In all mouse experiments, the morning of vaginal plug was designated embryonic day 0.5 (E0.5). Both
581 males and females were used.
582
583 **In utero electroporation**
584 In utero electroporation was performed as described previously [1] using the following plasmids:
585 pLKO.1-Cic shRNA (Sigma, TRCN0000304642; 5'-CCG GAG CGG GAG AAG GAC CAT ATT CCT
586 CGA GGA ATA TGG TCC TTC TCC CGC TTT TTT G-3'), pLKO.1-non-targeting shRNA (Sigma; 5'-
587 CCT AAG GTT AAG TCG CCC TCG CTC GAG CGA GGG CGA CTT AAC CTT AGG -3'), pCIG2-Cre
588 (which contains Cre-IRES-GFP), pCIC-ETV5 (which contains Etv5-IRES-mCherry), Super piggyBac
589 Transposase (Systems Biosciences, SBI), and piggyBac cargo vector PB513B-1 (SBI) into which
590 cDNAs were cloned for Turbo-Cre and Etv5. The DN-ETV5 consists of an *Etv5-EnR* fusion (gift of Dr.
591 Carol Schuurmans) cloned into the piggyBac construct modified to contain the CAG promoter and
592 GFP-luciferase. DNA was prepared with Endo-free DNA kit (Qiagen) and was injected at 1.5 µg/µl into
593 the telencephalic vesicles of embryos in time-staged pregnant females using a Femtojet 4i
594 microinjector (Eppendorf) then followed by electrical pulses (6 x 43 V, 950 ms interval) applied by
595 platinum tweezer-style electrodes (7 mm, Protech) using a BTX square wave generator (Harvard
596 Apparatus). Post-procedure, embryos were allowed to develop until the time of harvesting. EdU (50
597 mg/ml in PBS) was injected intraperitoneally into the pregnant dam 30 minutes prior to euthanasia.
598
599 **Neural stem cell culture**
600 The VZ of E15 brains were dissected, and tissue was dissociated to single cells using Accumax (EMD
601 Millipore). Cells were grown at 37°C, 5% CO_2 in low-adhesion tissue culture flasks (Sarstedt) in mouse
602 neural stem cell (mNSC) media consisting of NeuroCult Proliferation media (Stem Cell Technologies)
603 supplemented with heparin, epidermal growth factor (EGF 20 ng/mL; Peprotech), and fibroblast
604 growth factor (FGF 20 ng/mL; Peprotech). When spheres reached 100–200 µm in diameter, cells were
605 split using Accumax and re-plated at 20,000 cells/mL.
606

607 **Transfection of cultured cells**

608 1-4 x 10^6 dissociated cells were re-suspended in 100 µL of Amaxa Mouse NSC Nucleofector Solution
609 (VPG-1004, Lonza) with 5 µg of plasmid DNA. Nucleofection was performed with a Nucleofector II
610 Device (Amaxa) using the A-033 program. Cells were returned to mouse neural stem cell media for
611 further expansion/selection. For siRNA-mediated Etv5 knockdown, cells were transfected with 50
612 nM Etv5 or Etv4 ON-TARGET Plus SMARTpool siRNAs (Dharmacon) using Lipofectamine 3000
613 reagent per manufacturer's protocol. Cells were assayed 48hrs hours post-transfection.

614

615 **Trypan Assay**

616 150,000 cells were seeded per T25 flask in mNSC media and counted after 72 hours on a TC20 cell
617 counter (Biorad) using Trypan blue stain (Thermo). Both dead and live cells were counted.

618

619 **Paired cell assay**

620 Dissociated cells were plated at 1,000 cells/ml in mNSC media on dishes coated with CTS CELLstart
621 (Thermo). After 20 hrs, cells were fixed in 4% PFA and immunostained for Ki67. Pairs were scored as
622 symmetric proliferative if both daughter nuclei were Ki67+, symmetric differentiative if both were Ki67-,
623 and asymmetric if one nucleus was Ki67+ and the other Ki67-.

624

625 **Neural Colony-Forming Cell Assay**

626 Cells in semi-solid media were prepared using the Neurocult NCFC Assay Kit (Stem Cell
627 Technologies) per manufacturer's protocol. Cells were plated at a density of 1,650 cells/ml using 1.5
628 ml per 35 mm culture dish. Dishes were replenished after 7 days with 60 µl of neural stem cell
629 proliferation media supplemented with heparin, EGF, and FGF. Sphere number and size were scored
630 using a gridded scoring dish (Stem Cell Technologies). 8-cell aggregates were used as the cut-off for
631 scoring.

632

633 **Lineage-directed differentiation**

634 Neuronal Differentiation: NSCs were seeded in mNSC proliferation media (Stem Cell Technologies)
635 on coverslips coated with Poly-L-Ornitihine and Laminin. After 24 hrs, media was replaced with
636 Neurobasal Media, 2% B-27, 2mM GlutaMAX-I (Thermo). After 4 more days dibutyryl cAMP (Sigma)
637 was added daily to a final concentration of 0.5 mM.
638 Oligodendroglial Differentiation: NSCs were seeded on coverslips coated with Poly-L-Ornitihine and
639 Laminin. After 24 hrs, media was replaced with Neurobasal media, 2% B-27, GlutaMAX-I, 30 ng/mL
640 3,3',5-Triiodo-L-thyronine sodium (Sigma).
641 Astrocyte Differentiation: NSCs were seeded on coverslips coated with Geltrex (Thermo). After 24 hrs,
642 media was replaced with DMEM, 1% N2-Supplement, 2mM GlutaMAX-I, 1% FBS.
643
644 **Immunostaining**
645 Tissue was fixed overnight in 4% PFA, cryoprotected in 30% sucrose/PBS, and embedded in Tissue-
646 Tek O.C.T. (Sakura Finetek) prior to cutting 6 µm cryosections on Superfrost Plus slides (VWR).
647 Cultured cells grown on coverslips were fixed for 20 minutes in 4% PFA then rinsed in PBS.
648 Permeabilization was performed with 1× TBST (Tris-buffered saline: 25 mM Tris, 0.14 M NaCl, 0.1%
649 Triton X-100) for 15 min at room temperature (RT). 3% goat or horse serum in TBST x 30 min was
650 used for block. Primary antibodies applied for 1 hr at RT or O/N at 4°C in block. Alexa Fluor
651 secondary antibodies were applied at 1:500 dilution for 1 hour RT. Nuclei were counterstained in 4′,6-
652 diamidino-2-phenylindole (DAPI; Santa Cruz) and mounted with FluorSave Reagent (Calbiochem). For
653 immunostaining of tissue sections when two or more primary antibodies were from the same host
654 species and for comparison of cell-type specific CIC expression, the Opal 4-colour IHC kit (Perkin
655 Elmer) was used per manufacturer's protocol.
656
657 **Western blotting**
658 Cells/tissue was lysed in RIPA buffer (10 mM Tris-Cl pH 8, 1 mM EDTA, 1% Triton X-100, 0.1%
659 sodium deoxycholate, 0.1% SDS, 140 mM NaCl, 1 mM PMSF) with 1X Halt Protease and
660 Phosphatase Inhibitor Cocktail (Thermo). 20 µg protein lysate (50 µg in the case of CIC probing) was

661 run on 4-12% Bis-Tris or 3-8% Tris-Acetate gels (Thermo). Protein was transferred to PVDF
662 membranes in NuPAGE Transfer Buffer (Thermo). Membranes were blocked in TBST with 5%
663 powdered milk. Primary antibodies diluted were applied for 1 hr at room temperature or overnight at
664 4°C. Horseradish peroxidase-coupled secondary antibodies were applied for 1 hr at room
665 temperature. Membranes were developed using ECL Plus Western Blotting Reagent (GE Healthcare)
666 and X-ray film.
667
668 **Transcriptional analysis**
669 Total RNA was extracted using AllPrep DNA/RNA/Protein Mini Kit (Qiagen) per manufacturer's
670 protocol. For each of 3 biologic replicates per condition, 100 ng RNA was subjected to nanoString
671 analysis on nCounter system (NanoString Technologies) using a custom gene expression codeset
672 containing neurodevelopmental and brain cancer associated genes, and 3 housekeeping genes. Data
673 were analyzed using nSolver software and exported to PRISM software for further statistical analyses.
674 Counts for Etv1, Etv4, and Etv5 were normalized to the average of 3 house-keeping genes (GAPDH,
675 Actin, Tubulin beta chain).
676
677 ***In situ* hybridization**
678 Digoxygenin (DIG)-labeled riboprobes were prepared using a 10x DIG-labeling kit (Roche), and ISH
679 was performed as described previously using probes for *GFP* and *Etv5* (17).
680
681 **Chromatin immunoprecipitation**
682 50 mg P6 mouse forebrain tissue was use per ChIP assay. ChIP was performed with the SimpleChip
683 Plus Kit with magnetic beads (Cell Signaling) per manufacturer's protocol with the following
684 exceptions. Tissue was disaggregated using a Dounce homogenizer. In place of micrococcal
685 nuclease, shearing was performed on a UCD Bioruptor on high power with intervals of 30 seconds on,
686 1 minute off for 30 minutes. 1.5 µl of anti-CIC (PA1-46018, Thermo) was used per IP reaction. Histone
687 H3 antibody and normal rabbit IgG were used as positive and negative controls, as supplied in the kit.

688 PCR primers for the ETV5 promoter region were: 5′-GGTGCAGGCCGAGGCCAGGG-3′ (For) and 5′-
689 CATTGACCAATCAGCACCGG-3′ (Rev).
690
691 **Image Analysis**
692 Coronal sections at the level of the anterior commissure were used in all quantitations of cell
693 populations and staining intensities in the dorsal cerebral cortex and corpus callosum. Slides were
694 imaged on AxioObserver fluorescence microscope (Zeiss). Images were processed using CS6
695 Photoshop software (Adobe) for orientation, false colorization, and overlay/colocalization. Enumeration
696 of cells positive for cytoskeletal, cytoplasmic or membrane proteins was performed manually by
697 counting positive cells using the Photoshop CS6 counting tool. Quantitation of CIC nuclear staining
698 intensity and MBP staining density was performed using FIJI software (47) as follows. Images were
699 first processed using Gaussian blur, then background subtracted. Default threshold limits were used in
700 the threshold tool. Images were converted to binary and watershed was run to separate clumped
701 cells. Nuclear staining was quantitated by using the analysing particles option with separate cut-offs
702 set for each antibody used. For quantitation of MBP expression on tissue sections, FIJI was used by
703 drawing regions of interest on the lateral corpus callosum (cingulum), and the mean integrated density
704 in the regions of interest was calculated.
705

706 **Intracranial BTIC xenografts and Bioluminescence imaging**

707 BT88 oligodendroglioma cells were obtained from the Dr. S. Weiss, University of Calgary (33). 1×10^5
708 BT88 cells stably transfected with CIC-GFP-Luciferase or DNETV5-GFP or respective empty vectors
709 were stereotactically implanted into the right striata of 6- to 8-week-old NOD/SCID mice. 6 weeks post-
710 implantation, tumour burden was measured either by bioluminescence imaging using IVIS Spectrum
711 In Vivo Imaging System (Xenogen) and/or by histology from euthanized animals. Mice were
712 anaesthetized under isoflurane and intraperitoneal injection of XenoLight D-Luciferin (PerkinElmer)
713 was administered at a dose of 150mg/kg body weight. Acquisition of bioluminescence images was

714 performed 10 min post-injection. Analysis was performed using Living Image Software by
715 measurement of photon counts (photon/s/cm^2) with a region of interest drawn around the
716 bioluminescence signal.
717
718 **Statistics**
719 Data are represented as mean ± SD from at least 3 biologic replicates for experiments. Comparisons
720 between experimental and control samples were made using 2-tailed t-test or, when there were more
721 than 2 groups, using ANOVA. Tukey's procedure was applied post-hoc to correct for multiple
722 comparisons during multiple pairwise analyses (e.g. differential Cic expression among cell types).
723 Bonferroni post-hoc correction was applied for statistical analysis of data from NanoString assays.
724 Statistical analyses were performed using Prism sofware (Graphpad).
725
726 **Study Approval**
727 Animal use was approved by the University of Calgary Animal Care Committee (protocol AC16-0266)
728 in compliance with the Guidelines of the Canadian Council of Animal Care.
729
730 **Data Availability**
731 The data that support the findings in this study are available from the corresponding author upon
732 reasonable request.
733
734 **Availability of Biological Materials**
735 Biological materials used in this study are available from the corresponding author upon reasonable
736 request.
737
738 **AUTHOR CONTRIBUTIONS**
739 Conceptualization, JAC, STA; Methodology, JAC, CS, STA; Investigation, STA, ADR, RD, LF, MJC,
740 MA, WW, SOL; Acquisition, Analyses and Interpretation of data, JAC, STA; Writing – Original Draft,

741 JAC, STA; Writing – Review & Editing, JAC, SC, JGC, SMR, MAM, WW, RD, SOL; Funding
742 Acquisition, JAC, JGC, CS; Resources, LA, MA, CS; Supervision, JAC, CS, JGC, SMR.
743

744 **ACKNOWLEDGEMENTS**

745 This work was funded by Canadian Institutes for Health Research (JAC), Cancer Research Society
746 (CS, JAC), Alberta Cancer Foundation (STA, ADR, LF, JGC), Alberta Innovates Health Solutions
747 (JAC, CS).
748

749 **COMPETING FINANCIAL INTERESTS**

750 The authors have no competing financial interests to declare.
751
752

753 **REFERENCES**
754

755 1. Reifenberger G, Kros JM, Louis DN, and Collins VP. In: Louis DN, Ohgaki H, Wiestler OD,
756 and Cavenee WK eds. *WHO Classification of Tumours of the Central Nervous System*. Lyon:
757 International Agency for Research on Cancer (IARC); 2016:54-62.
758 2. Persson AI, Petritsch C, Swartling FJ, Itsara M, Sim FJ, Auvergne R, et al. Non-stem cell origin
759 for oligodendroglioma. *Cancer cell.* 2010;18(6):669-82.
760 3. Yip S, Butterfield YS, Morozova O, Chittaranjan S, Blough MD, An J, et al. Concurrent CIC
761 mutations, IDH mutations, and 1p/19q loss distinguish oligodendrogliomas from other cancers.
762 *The Journal of pathology.* 2012;226(1):7-16.
763 4. Bettegowda C, Agrawal N, Jiao Y, Sausen M, Wood LD, Hruban RH, et al. Mutations in CIC
764 and FUBP1 contribute to human oligodendroglioma. *Science.* 2011;333(6048):1453-5.
765 5. Cancer Genome Atlas Research N, Brat DJ, Verhaak RG, Aldape KD, Yung WK, Salama SR,
766 et al. Comprehensive, Integrative Genomic Analysis of Diffuse Lower-Grade Gliomas. *N Engl*
767 *J Med.* 2015;372(26):2481-98.
768 6. Jimenez G, Shvartsman SY, and Paroush Z. The Capicua repressor - a general sensor of RTK
769 signaling in development and disease. *Journal of cell science.* 2012;125(Pt 6):1383-91.
770 7. Lohr U, Chung HR, Beller M, and Jackle H. Antagonistic action of Bicoid and the repressor
771 Capicua determines the spatial limits of Drosophila head gene expression domains. *Proc Natl*
772 *Acad Sci U S A.* 2009;106(51):21695-700.
773 8. Ajuria L, Nieva C, Winkler C, Kuo D, Samper N, Andreu MJ, et al. Capicua DNA-binding sites
774 are general response elements for RTK signaling in Drosophila. *Development.*
775 2011;138(5):915-24.
776 9. Grimm O, Zini VS, Kim Y, Casanova J, Shvartsman SY, and Wieschaus E. Torso RTK controls
777 Capicua degradation by changing its subcellular localization. *Development.* 2012;139(21):3962-
778 8.
779 10. Astigarraga S, Grossman R, Diaz-Delfin J, Caelles C, Paroush Z, and Jimenez G. A MAPK
780 docking site is critical for downregulation of Capicua by Torso and EGFR RTK signaling. *The*
781 *EMBO journal.* 2007;26(3):668-77.
782 11. Lim B, Samper N, Lu H, Rushlow C, Jimenez G, and Shvartsman SY. Kinetics of gene
783 derepression by ERK signaling. *Proc Natl Acad Sci U S A.* 2013;110(25):10330-5.
784 12. Dissanayake K, Toth R, Blakey J, Olsson O, Campbell DG, Prescott AR, et al.
785 ERK/p90(RSK)/14-3-3 signalling has an impact on expression of PEA3 Ets transcription
786 factors via the transcriptional repressor capicua. *The Biochemical journal.* 2011;433(3):515-25.
787 13. Yang R, Chen LH, Hansen LJ, Carpenter AB, Moure CJ, Liu H, et al. Cic Loss Promotes
788 Gliomagenesis via Aberrant Neural Stem Cell Proliferation and Differentiation. *Cancer Res.*
789 2017;77(22):6097-108.
790 14. Lu HC, Tan Q, Rousseaux MW, Wang W, Kim JY, Richman R, et al. Disruption of the
791 ATXN1-CIC complex causes a spectrum of neurobehavioral phenotypes in mice and humans.
792 *Nature genetics.* 2017;49(4):527-36.
793 15. Graham V, Khudyakov J, Ellis P, and Pevny L. SOX2 functions to maintain neural progenitor
794 identity. *Neuron.* 2003;39(5):749-65.
795 16. Faedo A, Borello U, and Rubenstein JL. Repression of Fgf signaling by sprouty1-2 regulates
796 cortical patterning in two distinct regions and times. *The Journal of neuroscience : the official*
797 *journal of the Society for Neuroscience.* 2010;30(11):4015-23.
798 17. Li S, Mattar P, Dixit R, Lawn SO, Wilkinson G, Kinch C, et al. RAS/ERK signaling controls
799 proneural genetic programs in cortical development and gliomagenesis. *The Journal of*
800 *neuroscience : the official journal of the Society for Neuroscience.* 2014;34(6):2169-90.

801 18. Kriegstein A, and Alvarez-Buylla A. The glial nature of embryonic and adult neural stem cells.
802 *Annual review of neuroscience.* 2009;32:149-84.
803 19. Lim DA, and Alvarez-Buylla A. The Adult Ventricular-Subventricular Zone (V-SVZ) and
804 Olfactory Bulb (OB) Neurogenesis. *Cold Spring Harb Perspect Biol.* 2016;8(5).
805 20. Lu QR, Sun T, Zhu Z, Ma N, Garcia M, Stiles CD, et al. Common developmental requirement
806 for Olig function indicates a motor neuron/oligodendrocyte connection. *Cell.* 2002;109(1):75-
807 86.
808 21. Zhou Q, Choi G, and Anderson DJ. The bHLH transcription factor Olig2 promotes
809 oligodendrocyte differentiation in collaboration with Nkx2.2. *Neuron.* 2001;31(5):791-807.
810 22. Fores M, Simon-Carrasco L, Ajuria L, Samper N, Gonzalez-Crespo S, Drosten M, et al. A new
811 mode of DNA binding distinguishes Capicua from other HMG-box factors and explains its
812 mutation patterns in cancer. *PLoS genetics.* 2017;13(3):e1006622.
813 23. Jimenez G, Guichet A, Ephrussi A, and Casanova J. Relief of gene repression by torso RTK
814 signaling: role of capicua in Drosophila terminal and dorsoventral patterning. *Genes &*
815 *development.* 2000;14(2):224-31.
816 24. Lee CJ, Chan WI, Cheung M, Cheng YC, Appleby VJ, Orme AT, et al. CIC, a member of a
817 novel subfamily of the HMG-box superfamily, is transiently expressed in developing granule
818 neurons. *Brain Res Mol Brain Res.* 2002;106(1-2):151-6.
819 25. Kawamura-Saito M, Yamazaki Y, Kaneko K, Kawaguchi N, Kanda H, Mukai H, et al. Fusion
820 between CIC and DUX4 up-regulates PEA3 family genes in Ewing-like sarcomas with
821 t(4;19)(q35;q13) translocation. *Human molecular genetics.* 2006;15(13):2125-37.
822 26. Hebert JM, and McConnell SK. Targeting of cre to the Foxg1 (BF-1) locus mediates loxP
823 recombination in the telencephalon and other developing head structures. *Developmental*
824 *biology.* 2000;222(2):296-306.
825 27. Sugiarto S, Persson AI, Munoz EG, Waldhuber M, Lamagna C, Andor N, et al. Asymmetry-
826 defective oligodendrocyte progenitors are glioma precursors. *Cancer cell.* 2011;20(3):328-40.
827 28. Finzsch M, Stolt CC, Lommes P, and Wegner M. Sox9 and Sox10 influence survival and
828 migration of oligodendrocyte precursors in the spinal cord by regulating PDGF receptor alpha
829 expression. *Development.* 2008;135(4):637-46.
830 29. Kang P, Lee HK, Glasgow SM, Finley M, Donti T, Gaber ZB, et al. Sox9 and NFIA coordinate
831 a transcriptional regulatory cascade during the initiation of gliogenesis. *Neuron.* 2012;74(1):79-
832 94.
833 30. Stolt CC, Lommes P, Sock E, Chaboissier MC, Schedl A, and Wegner M. The Sox9
834 transcription factor determines glial fate choice in the developing spinal cord. *Genes &*
835 *development.* 2003;17(13):1677-89.
836 31. Lee Y, Fryer JD, Kang H, Crespo-Barreto J, Bowman AB, Gao Y, et al. ATXN1 protein family
837 and CIC regulate extracellular matrix remodeling and lung alveolarization. *Developmental cell.*
838 2011;21(4):746-57.
839 32. Padul V, Epari S, Moiyadi A, Shetty P, and Shirsat NV. ETV/Pea3 family transcription factor-
840 encoding genes are overexpressed in CIC-mutant oligodendrogliomas. *Genes Chromosomes*
841 *Cancer.* 2015;54(12):725-33.
842 33. Crespo-Barreto J, Fryer JD, Shaw CA, Orr HT, and Zoghbi HY. Partial loss of ataxin-1 function
843 contributes to transcriptional dysregulation in spinocerebellar ataxia type 1 pathogenesis. *PLoS*
844 *genetics.* 2010;6(7):e1001021.
845 34. Li X, Newbern JM, Wu Y, Morgan-Smith M, Zhong J, Charron J, et al. MEK Is a Key
846 Regulator of Gliogenesis in the Developing Brain. *Neuron.* 2012;75(6):1035-50.
847 35. Kelly JJ, Blough MD, Stechishin OD, Chan JA, Beauchamp D, Perizzolo M, et al.
848 Oligodendroglioma cell lines containing t(1;19)(q10;p10). *Neuro Oncol.* 2010;12(7):745-55.

849 36. Davoli T, Xu AW, Mengwasser KE, Sack LM, Yoon JC, Park PJ, et al. Cumulative
850 haploinsufficiency and triplosensitivity drive aneuploidy patterns and shape the cancer genome.
851 *Cell.* 2013;155(4):948-62.
852 37. Lam YC, Bowman AB, Jafar-Nejad P, Lim J, Richman R, Fryer JD, et al. ATAXIN-1 interacts
853 with the repressor Capicua in its native complex to cause SCA1 neuropathology. *Cell.*
854 2006;127(7):1335-47.
855 38. Rousseaux MWC, Tschumperlin T, Lu HC, Lackey EP, Bondar VV, Wan YW, et al. ATXN1-
856 CIC Complex Is the Primary Driver of Cerebellar Pathology in Spinocerebellar Ataxia Type 1
857 through a Gain-of-Function Mechanism. *Neuron.* 2018;97(6):1235-43 e5.
858 39. Cairncross G, and Jenkins R. Gliomas with 1p/19q codeletion: a.k.a. oligodendroglioma.
859 *Cancer J.* 2008;14(6):352-7.
860 40. Shoshan Y, Nishiyama A, Chang A, Mork S, Barnett GH, Cowell JK, et al. Expression of
861 oligodendrocyte progenitor cell antigens by gliomas: implications for the histogenesis of brain
862 tumors. *Proc Natl Acad Sci U S A.* 1999;96(18):10361-6.
863 41. Liu C, Sage JC, Miller MR, Verhaak RG, Hippenmeyer S, Vogel H, et al. Mosaic analysis with
864 double markers reveals tumor cell of origin in glioma. *Cell.* 2011;146(2):209-21.
865 42. Butler MS, Roshan-Moniri M, Hsing M, Lau D, Kim A, Yen P, et al. Discovery and
866 characterization of small molecules targeting the DNA-binding ETS domain of ERG in prostate
867 cancer. *Oncotarget.* 2017;8(26):42438-54.
868 43. Pop MS, Stransky N, Garvie CW, Theurillat JP, Hartman EC, Lewis TA, et al. A small
869 molecule that binds and inhibits the ETV1 transcription factor oncoprotein. *Mol Cancer Ther.*
870 2014;13(6):1492-502.
871 44. Wang X, Qiao Y, Asangani IA, Ateeq B, Poliakov A, Cieslik M, et al. Development of
872 Peptidomimetic Inhibitors of the ERG Gene Fusion Product in Prostate Cancer. *Cancer cell.*
873 2017;31(4):532-48 e7.
874 45. Pirozzi CJ, Carpenter AB, Waitkus MS, Wang CY, Zhu H, Hansen LJ, et al. Mutant IDH1
875 Disrupts the Mouse Subventricular Zone and Alters Brain Tumor Progression. *Mol Cancer Res.*
876 2017.
877 46. Tirosh I, Venteicher AS, Hebert C, Escalante LE, Patel AP, Yizhak K, et al. Single-cell RNA-
878 seq supports a developmental hierarchy in human oligodendroglioma. *Nature.*
879 2016;539(7628):309-13.
880 47. Schindelin J, Arganda-Carreras I, Frise E, Kaynig V, Longair M, Pietzsch T, et al. Fiji: an open-
881 source platform for biological-image analysis. *Nat Methods.* 2012;9(7):676-82.

882

883

884 **FIGURES**
885

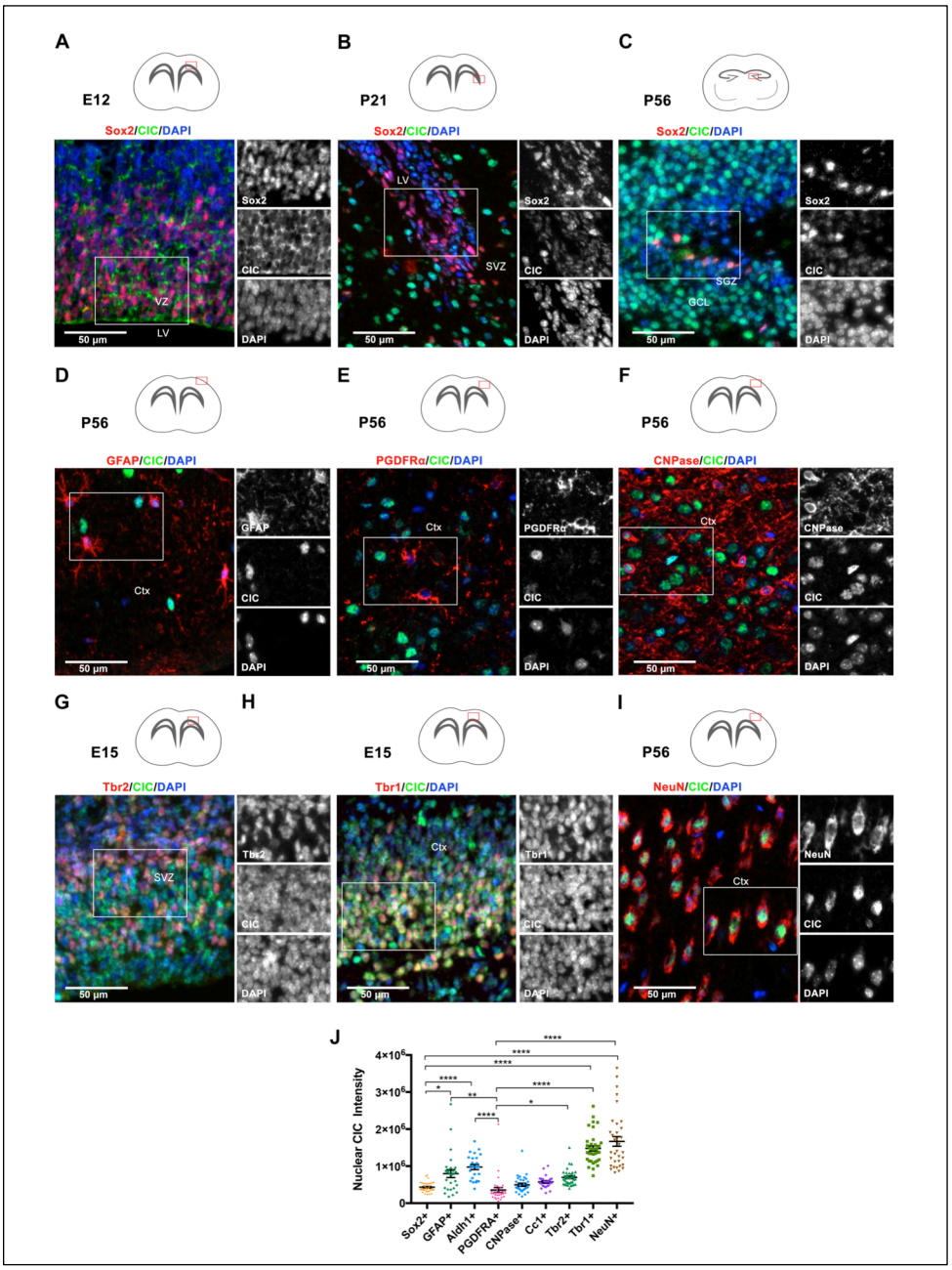

904 **FIGURE 1: Differential Cic expression among cell types in the developing and mature brain.**
905 Representative images of immunofluorescence staining for Cic expression in Sox2+ stem cell populations in (A)
906 E12 subventricular zone, (B) P56 hippocampal dentate gyrus subgranular zone, and (C) P56 subventricular
907 zone. Cic expression in glial cells in the adult brain showing localization in (D) Gfap+ cortical astrocytes, (E)
908 Pdgfra+ white matter OPCs, and (F) CNPase+ mature oligodendrocytes. Cic expression in cortical neuronal
909 populations (G) E15 Tbr2+ early-born neurons in the SVZ and IZ, (H) E15 Tbr1+ late-born neurons in the cortical
910 plate, and (I) adult post-mitotic NeuN+ cortical neurons. (J) Quantitation of Cic nuclear staining intensities,
911 plotted for different brain cell types. Each point represents one cell quantitated. Results show quantitation from a
912 minimum of 24 cells per marker from the boxed regions used for image analysis. All quantitation performed on
913 P56 cortex except Tbr2 and Tbr1 which were analyzed at E15. Pairwise comparisons between cell types
914 performed by ANOVA with Tukey's posthoc test. Data shown as mean ± SD. *$p<0.05$, **$p<0.01$, ****$p<0.0001$.
915 LV–lateral ventricle, GCL–granule cell layer, SGZ–subgranular zone, SVZ–subventricular zone, Ctx–cortex.

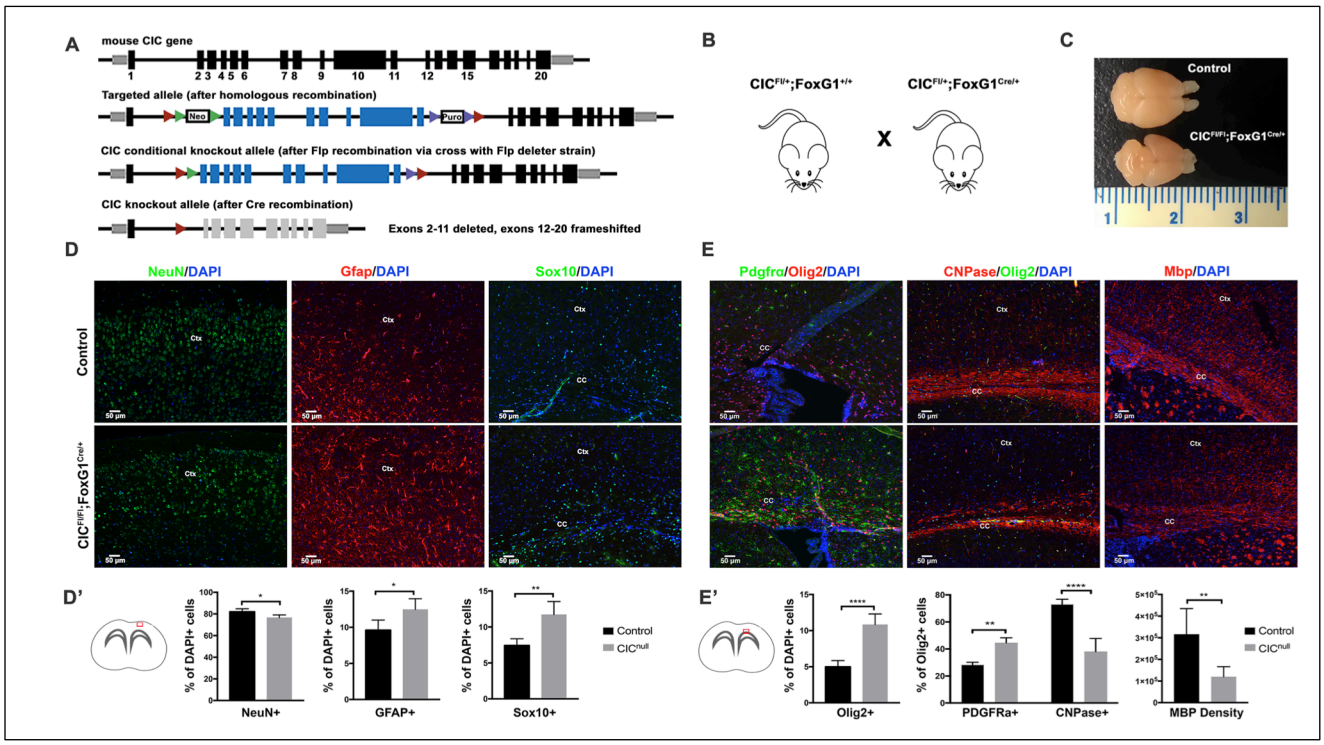

FIGURE 2: Forebrain-specific *Cic* deletion increases glial cells at the expense of neurons by P21 (A) Targeting strategy for Cic conditional knockout mice. Exon numbering is shown relative to Cic transcript variant 1. (B) Forebrain-deletion of Cic starting from E10.5 by crossing CIC-floxed line with FoxG1-cre. *Cic*$^{Fl/Fl}$*;FoxG1*$^{Cre/+}$ animals are compared with *Cic*$^{Fl/+}$*;FoxG*$^{Cre/+}$ or *Cic*$^{Fl/Fl}$*;FoxG1*$^{+/+}$ as controls. (C) Representative gross morphology of *Cic*-deleted and *Cic*-wildtype brains at P21. (D,D') Staining and quantitation of NeuN+, Gfap+, and Sox10+ cells in Cic-deleted (*Cic*$^{Fl/Fl}$*;FoxG1*$^{Cre/+}$) cortex vs control (*Cic*$^{Fl/Fl}$*;FoxG1*$^{+/+}$). (E,E') Staining and quantitation of Olig2+, Pdgfra+, and CNPase+ cells in lateral corpus callosum, and Mbp expression in lateral corpus callosum at P21. Results show quantitation from 5 mice per each group. Statistical analyses performed by unpaired t-test. Data shown as mean ± SD. *p<0.05, **p<0.01, ****p<0.0001. Ctx–cortex, CC–corpus callosum.

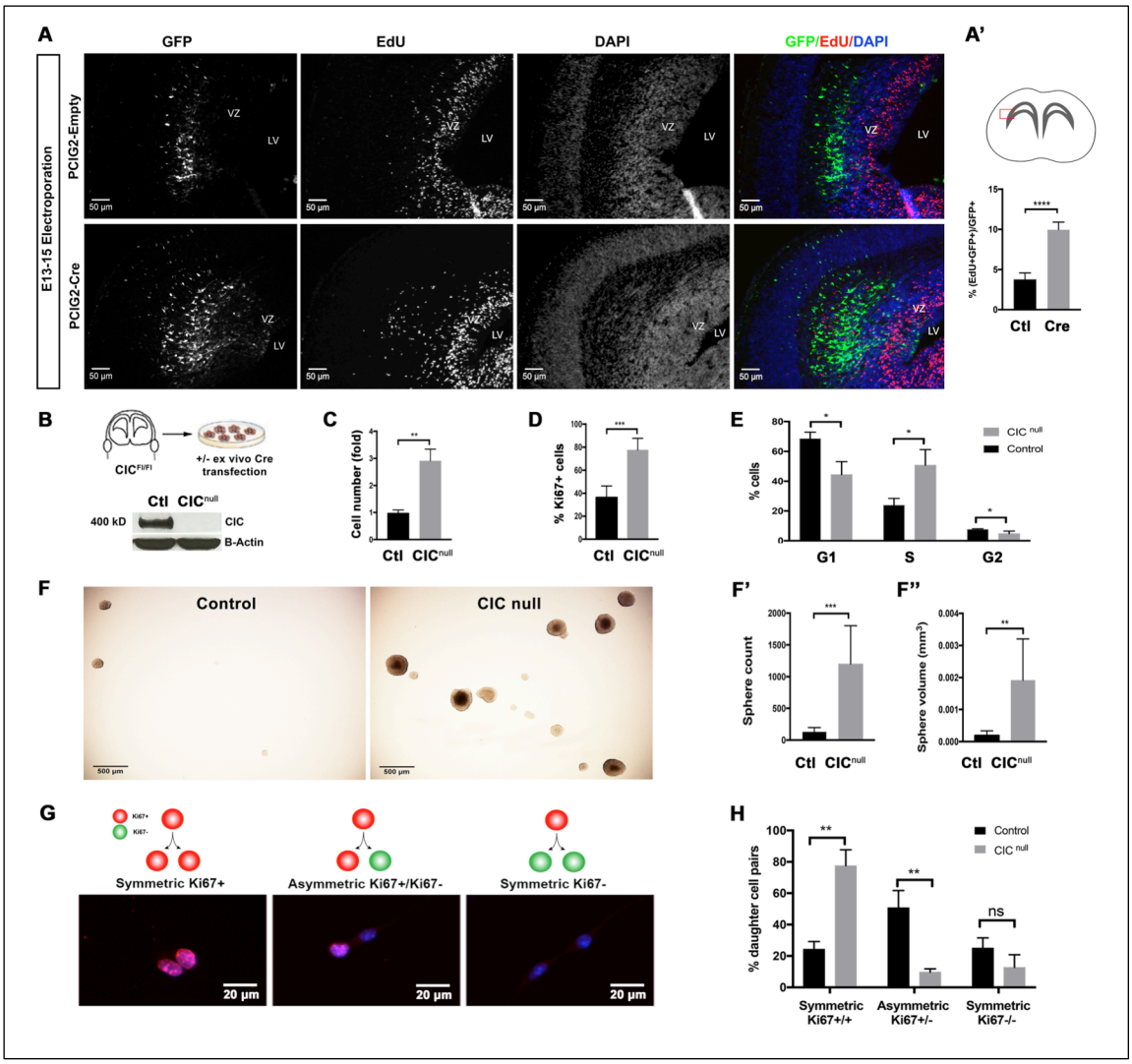

FIGURE 3: Cic deficiency increases proliferation and self-renewal of neural stem/progenitor cells. (A,A') EdU incorporation 48-hours after electroporation of *Cre* or control plasmid into VZ of E13 *Cic*-floxed embryos; boxed area indicates zone for imaging and quantitation (n ≥ 4 mice per group). (B) Generation of Cic-null cells and control cells from *Cic*-floxed cells via ex vivo transfection of Cre recombinase, and western blotting for validation of knockout. (C) Trypan blue assay, (D) Ki67 proliferation index, and (E) propidium iodide cell cycle analysis in cultured cells. (F) Neural colony forming assay with quantitation of (F') sphere number and (F'') sphere size. (G) Paired cell assay schematic and representative images with Ki67 immunostaining and (H) Quantitation of symmetric proliferative, asymmetric, and symmetric terminal divisions. Data shown as mean ± SD. Data from ≥ 3 biologic replicates per condition. Statistical analysis performed by unpaired t-test. ns-not significant, *p<0.05, **p<0.01, ***p<0.001, ****p<0.0001. VZ–ventricular zone, LV–lateral ventricle.

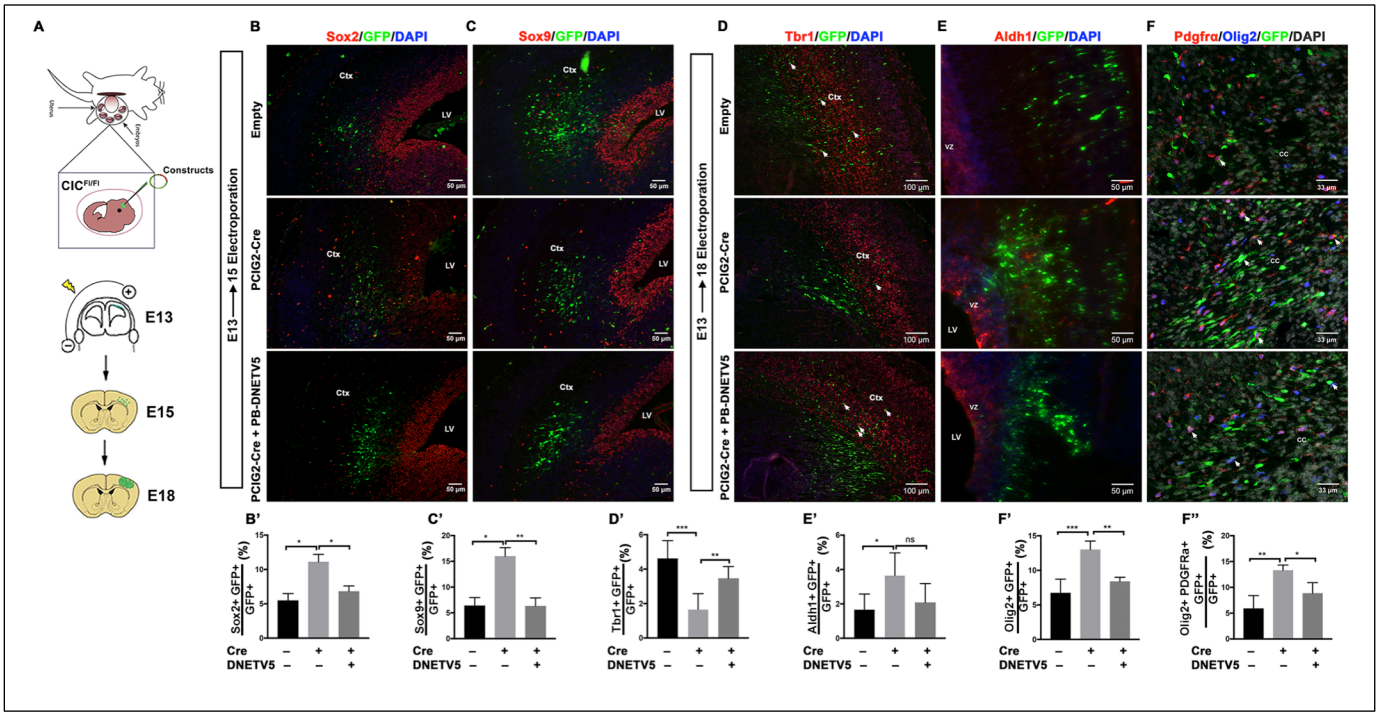

FIGURE 4: Deletion of *Cic* in the neurogenic period biases neural stem/progenitor cells to glial lineage selection. (A) Localized deletion of *Cic* in neural stem cells via *in-utero* electroporation into VZ cell of *C*ic-floxed embryos. Targeted cells carry a fluorescent marker and express either cre recombinase (Cre), dominant negative ETV5 (DNETV5), or not (Empty control), depending on the electroporated plasmid. Staining and quantitation of Sox2+ stem cells (B,B') and Sox9+ glioblasts (C,C') 2 days after E13 electroporation. Staining and quantitation of late-born Tbr1+ neurons, Aldh1+ astrocytes, Olig2+ oligodendrogial lineage cells, and Pdgfra+ oligodendrocyte precursors cells 5 days after E13 electroporation. Results show quantitation from 4 mice per group. Statistical analyses between control and experimental groups performed by ANOVA with Tukey's posthoc test. Data shown as mean ± SD. *p<0.05, **p<0.01, ***p<0.001, ns–not significant. Ctx–cortex, LV–lateral ventricle, VZ–ventricular zone.

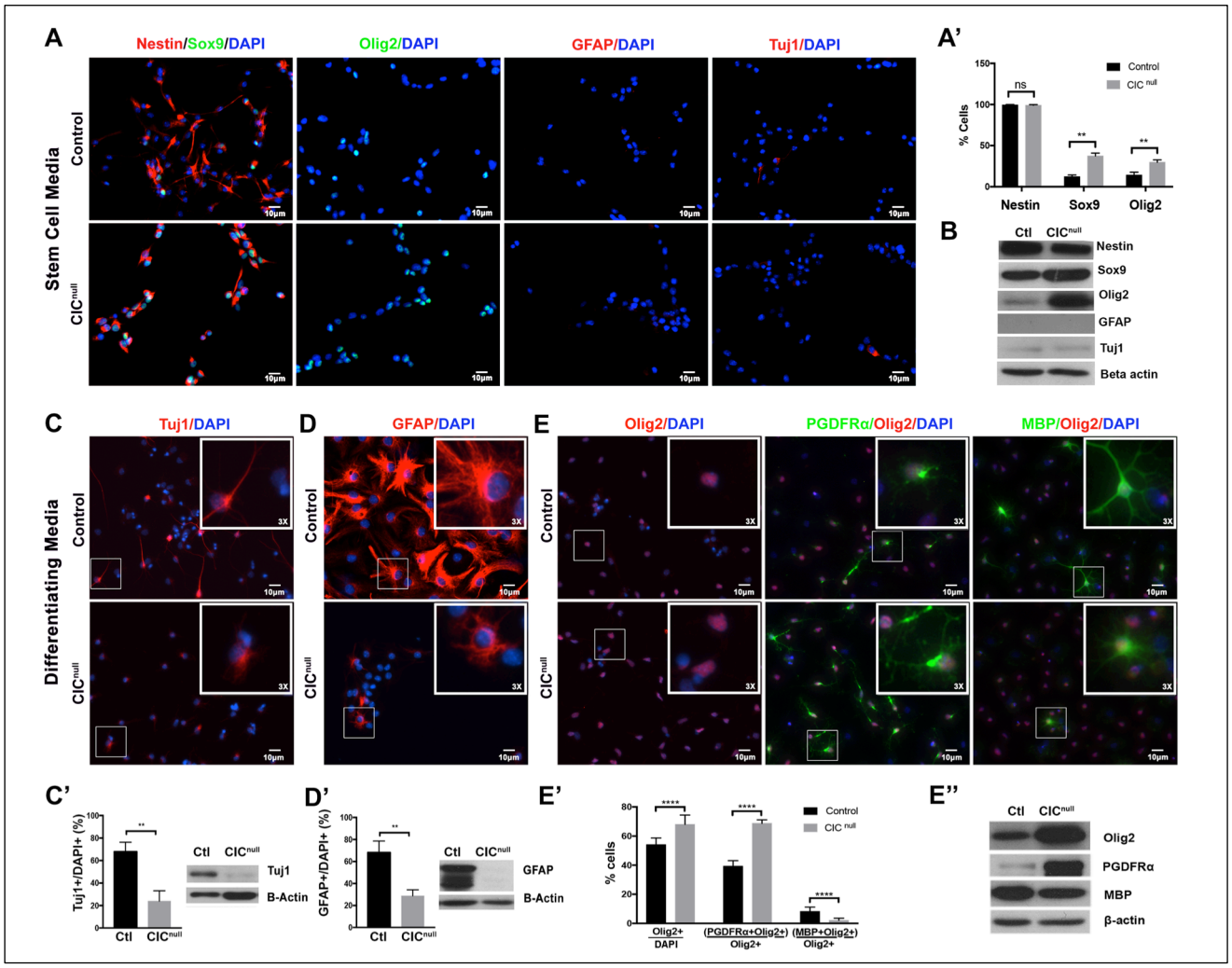

FIGURE 5: Cultured Cic null cells are oligodendrocyte lineage-biased. (A) Immunofluorescence and (B) Western blotting for Nestin, Sox9, Olig2, Gfap, and Tuj1 in Cic-null and control cells cultured in stem cell conditions. Responses of Cic-null and control cells to 10-day exposure to lineage-directed differentiation conditions for (C) neurons, (D) astrocytes, or (E) oligodendrocytes. Immunofluorescence quantitation of cell populations and western blotting of cells cultured in lineage-directed differentiation conditions for (C') neurons, (D') astrocytes, and (E', E'') stages of oligodendrocyte development. Data shown as mean ± SD. Data from ≥ 3 biologic replicates per condition. Statistical analysis performed by unpaired t-test. ns-not significant, **p<0.01, ****p<0.0001.

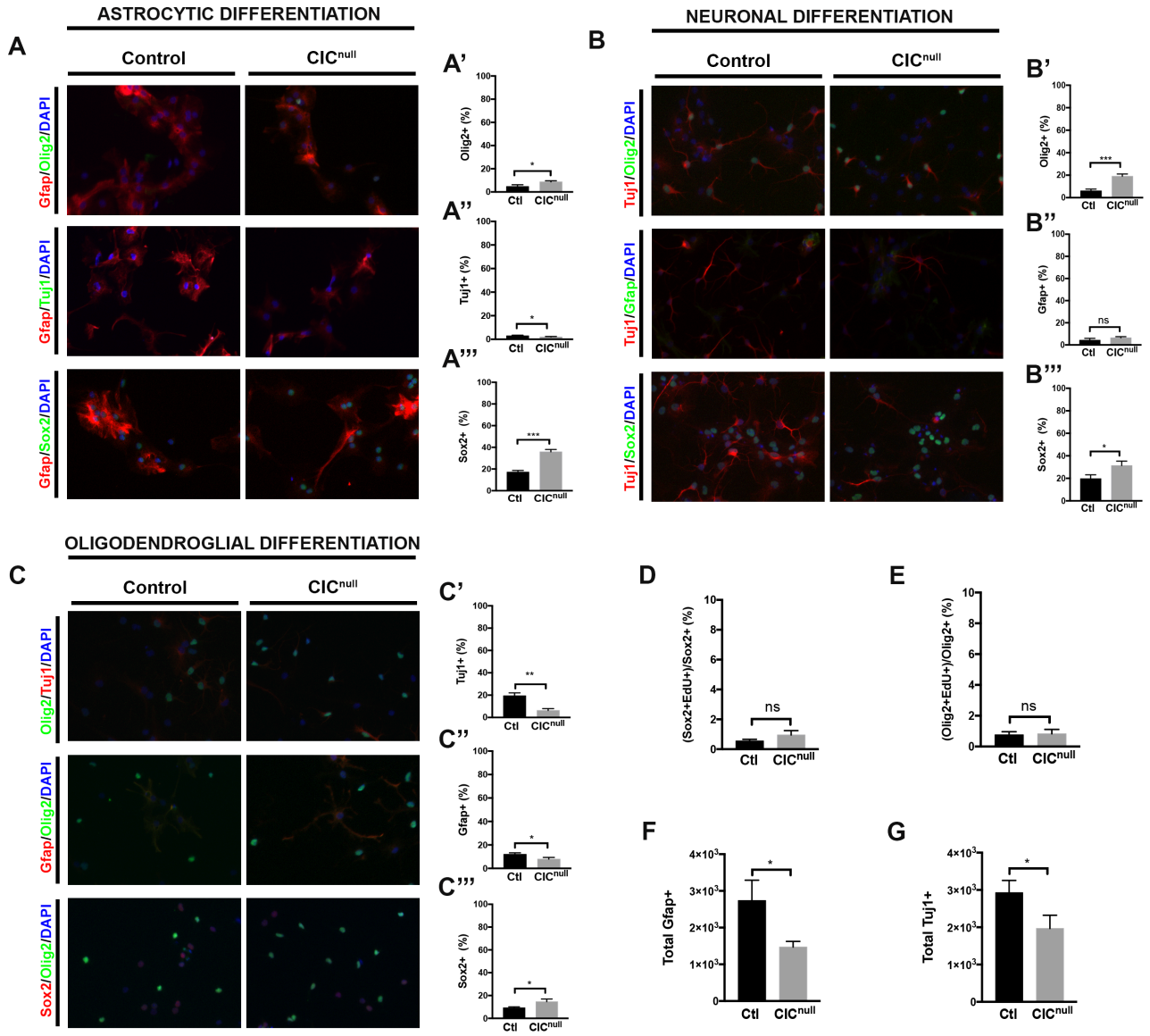

Figure 6: Alternate lineage selection of Cic null NSCs in response to extrinsic differentiation cues. (A) Under astrocytic promoting conditions, representative images of cultures stained for oligodendrocytes (Olig2+), neurons (Tuj1+) and stem cells (Sox2+); and (A',A'',A''') corresponding quantifications. (B) Under neuronal promoting conditions, representative images of cultures stained for oligodendrocytes (Olig2+), astrocytes (Gfap+) and stem cells (Sox2+); and (B',B'',B''') corresponding quantifications.(C) Under oligodendrocytic promoting conditions, representative images of cultures stained for neurons (Tuj1+), astrocytes (Gfap+) and stem cells (Sox2+); and (C',C'',C''') corresponding quantifications. (D) Percentage of Sox2+ cells positive for Edu incorporation after 10 days exposure to neuronal promoting conditions. (E) Percentage of Olig2+ positive for Edu incorporation after 10 days exposure to neuronal promoting conditions. (F) Absolute counts of Gfap+ cells/well after differentiating $4x10^3$ NSCs in astrocytic conditions for 10 days. (G) Absolute counts of Tuj1+ cells/well after differentiation $4x10^3$ NSCs in neuronal conditions for 10 days. Bars indicate mean±SD. ADC-Astrocytic differentiation condition, NDC-Neuronal differentiation condition, ODC-Oligodendroglial differentiation condition. ns – not significant, * $p<0.05$, ***$p<0.001$.

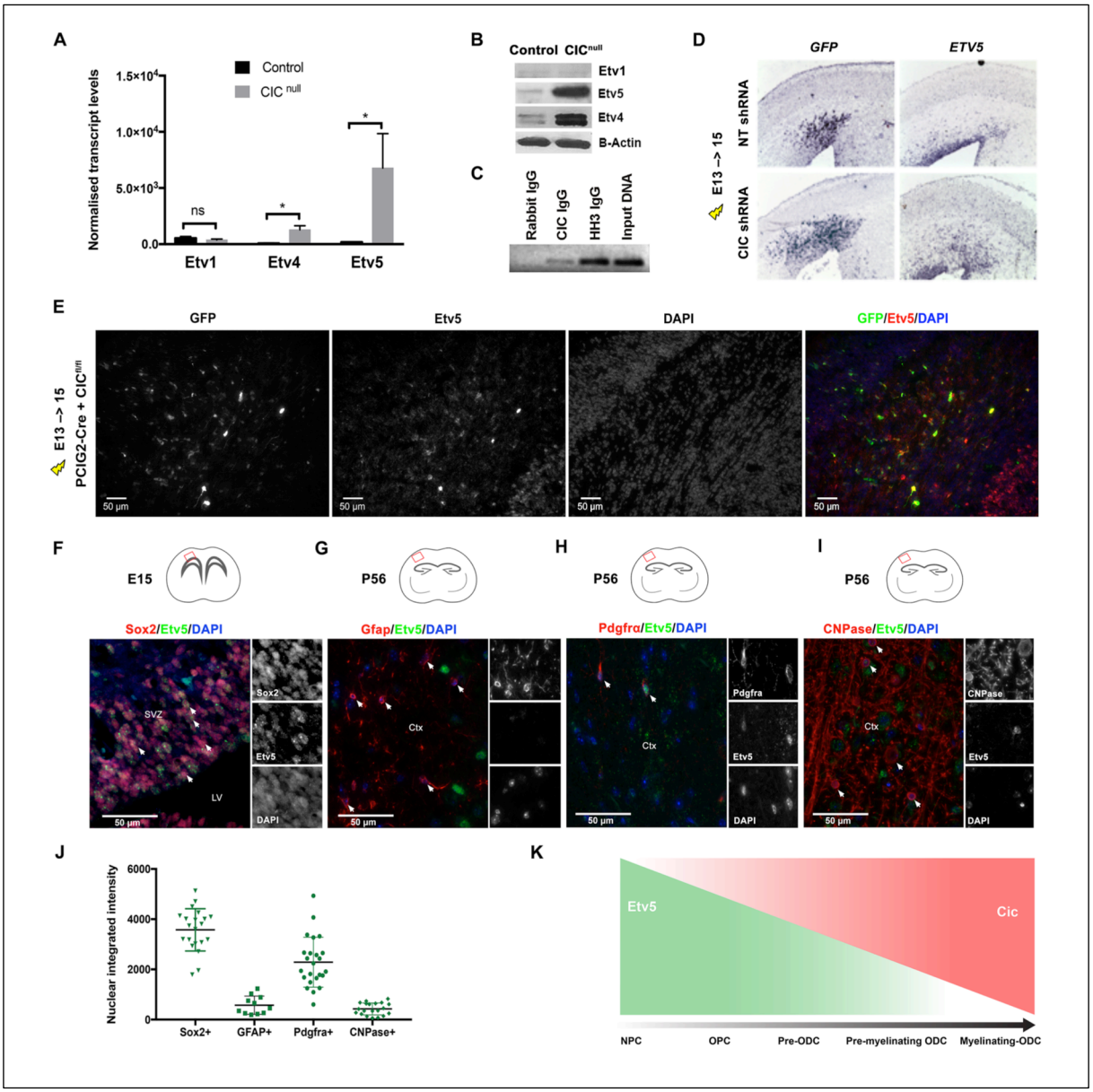

FIGURE 7: *Etv5* is a direct target of Cic transcriptional repression. *Etv1*, *Etv4*, and *Etv5* mRNA (A) and protein (B) levels in cultured CIC-null and -control cells after 48-hour exposure to oligodendrocytic differentiating conditions; transcript levels normalized to average of 3 (Actin, GAPDH, Tubulin beta chain) housekeeping genes. Data from n=3 biologic replicates. (C) ChIP-PCR for Cic at the *Etv5* promoter. (D) Electroporation of Cic shRNA or non-targeting (NT*)* shRNA at E13 followed by *in-situ* hybridization for *Etv5* and *GFP* at E15; *Etv5* transcripts are upregulated in areas of Cic knockdown. Data from n≥3 mice per group. (E) Immunofluorescence staining showing Etv5 and GFP protein expression 2 days after Cre electroporation into E13 VZ of *Cic*-floxed embryos. *Cic* deleted cells show increased Etv5 protein. (F-I, J) Differential Etv5 expression in (F) NSCs (Sox2+) at mid-neurogenesis, and in (G) astrocytes (Gfap+), (H) OPCs (Pdgfra+), and (I) mature oligodendrocytes (CNPase+) in P56 adult cortex. Each point represents one cell quantitated. Results show quantitation from ≥20 cells for each marker. Data shown as mean ± SD. Statistical analyses performed by unpaired t-test. *p<0.05. SVZ–subventricular zone, LV–lateral ventricle, Ctx–cortex. (K) Schematic depiction of relationship of Cic and Etv5 expression as neural stem cells differentiate to mature myelinating oligodendrocytes.

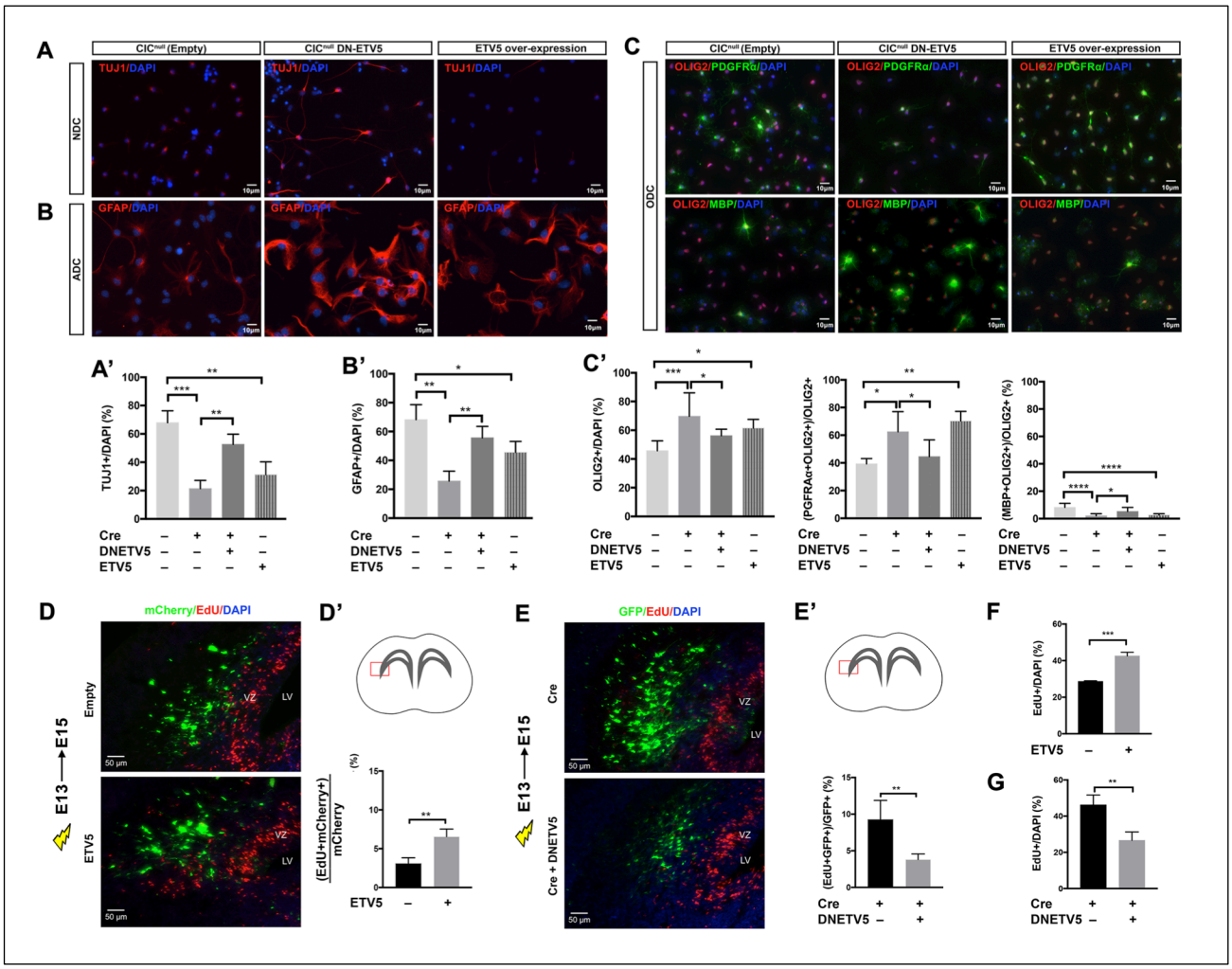

FIGURE 8: Etv5 is necessary and sufficient for proliferation and cell fate bias effects downstream of Cic loss. Cic-null cells with and without DN-ETV5, and Cic-wildtype cells with Etv5 overexpression were assessed for their ability to differentiate in response to 10-days' exposure to lineage-directed differentiating conditions. (A,A') Neuronal differentiation capacity was assessed by bIII-Tubulin immunostaining (Tuj1 positivity), (B,B') astrocytic differentiation capacity was assessed by Gfap immunostaining, and (C,C') oligodendroglial differentiation capacity was assess by staining for Olig2, Pdgfra, and Mbp. (D,D') EdU incorporation 2 days post-electroporation of wildtype *ETV5* or empty control plasmid, both carrying mCherry as a marker, into E13 $CIC^{Fl/Fl}$ VZ. Note: mCherry fluorescence and EdU staining were false-colorized to green and red after grayscale imaging. (E,E') EdU incorporation 2 days post-electroporation of Cre only or of Cre co-electroporated with *DN-ETV5* into E13 $CIC^{Fl/Fl}$ VZ . EdU incorporation assay in cultured NSCs showing (F) effects of ETV5 overexpression in CIC-wildtype NSCs and (G) effects of *DN-ETV5* expression in Cic-null NSCs. Data shown as mean ± SD from n ≥ 4 mice per each group for in vivo studies and n=3 biological replicates for cell culture studies. Statistical analyses performed either t-test in D', E', F, G; or with ANOVA with Tukey's posthoc test in A', B', C'. ns-not significant, *p<0.05, **p<0.01, ***p<0.0001. ADC–astrocytic differentiation condition, NDC–neuronal differentiation condition, ODC–oligodendrocytic differentiation condition. VZ–ventricular zone, LV–lateral ventricle.

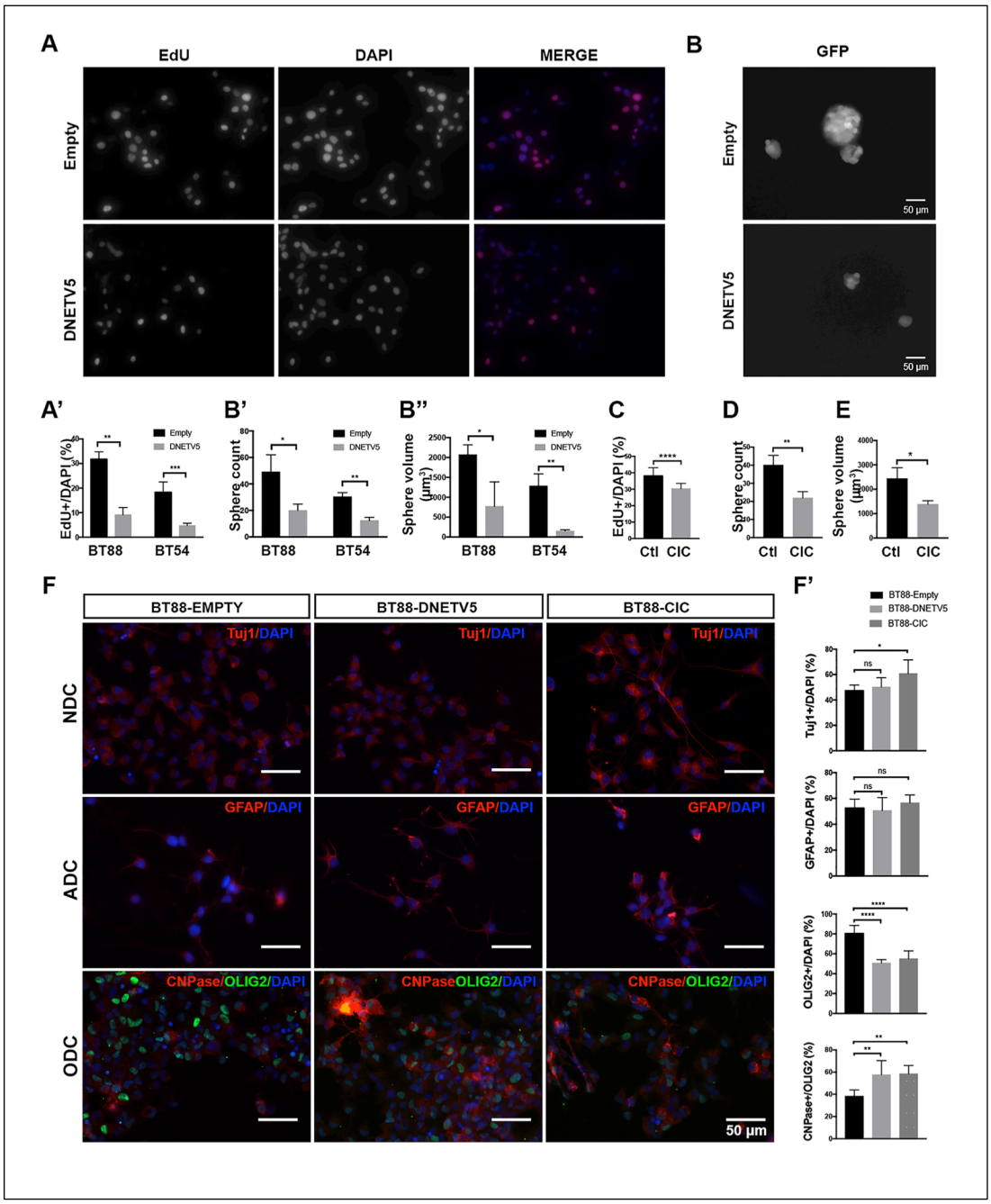

FIGURE 9: ODG cells require CIC loss or elevated ETV5 to maintain proliferation and stemness. (A,A') EdU incorporation in BT-88 and BT-54 ODG cell lines stably transfected with control plasmid or of DNETV5. Quantitation shows results from both cell lines. Representative images are from BT-88. (B) Representative images showing effect of DN-ETV5 on sphere formation in BT88 ODG cells. Quantification of (B') sphere number and (B") size in BT-54 and BT-88 ODG cells without and with DNETV5. (C,D,E) CIC re-expression in BT-88 cells decreases proliferation, sphere number, and sphere size. (F,F') Lineage-specific differentiation capacity of BT-88 ODG cells stably transfected with either control plasmid, DNETV5, or CIC; expression of Tuj1, GFAP, OLIG2, and CNPase after 10-days exposure to differentiation conditions for neurons, astrocytes, and oligodendrocytes. Data shown as mean ± SD from n=3 biologic replicates. Statistical analyses by ANOVA with Tukey's posthoc test. ns-not significant, *p<0.05, **p<0.01, ****p<0.0001. NDC–neuronal differentiation condition, ADC–astrocytic differentiation condition, ODC–oligodendrocytic differentiation condition.

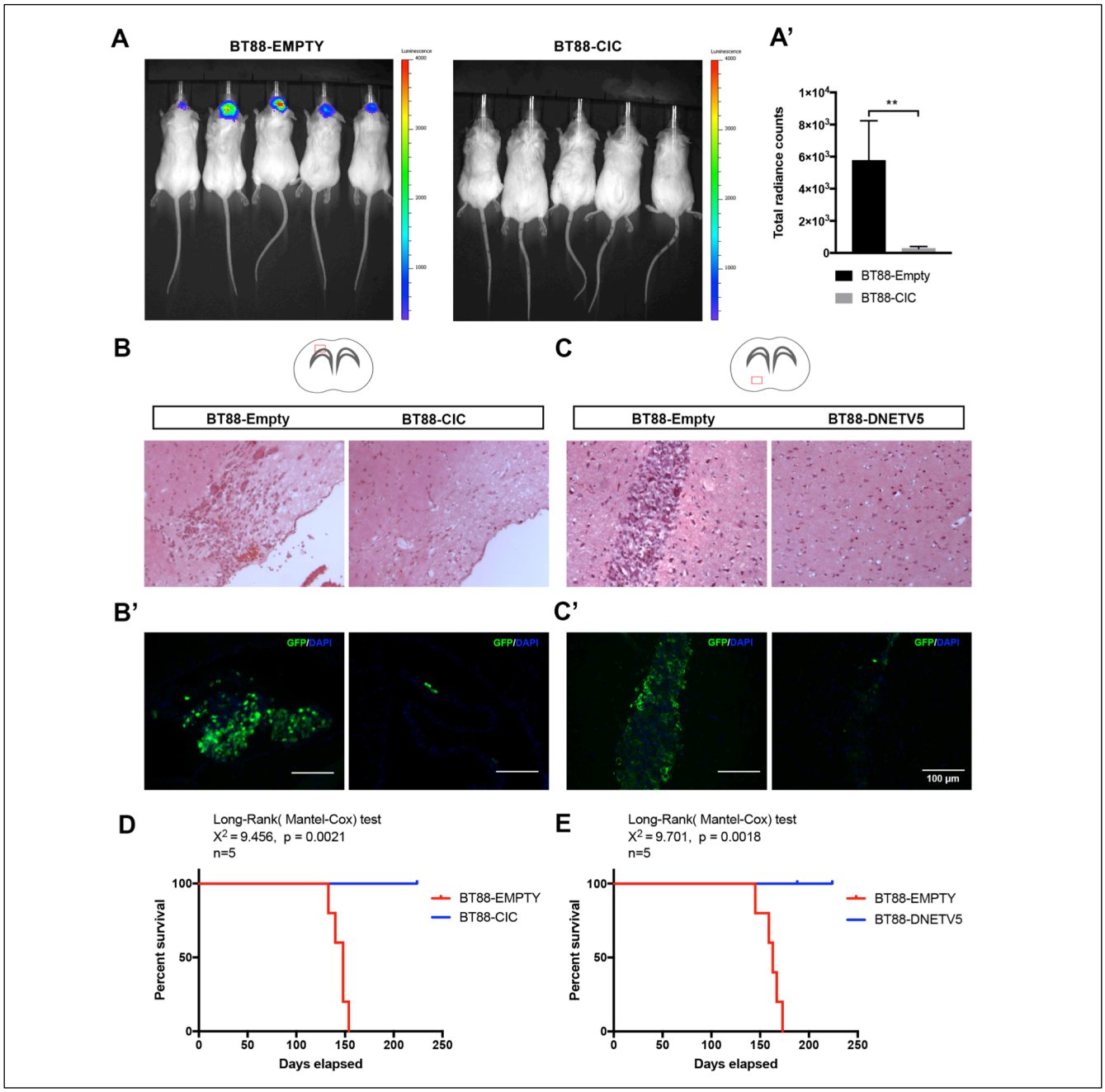

FIGURE 10: Tumorigenicity of ODG cells is reduced by CIC re-expression or ETV5 blockade. (A, A') Bioluminescence imaging of NOD-SCID mice at 6 weeks post-implantation of BT88 oligodendroglioma cells stably transfected with either empty-GFP-luciferase or CIC-GFP-luciferase expression vectors. Data shown as mean ± SD from 8 mice per group. Statistical analyses by student's t test. **p<0.01. (B,B') Representative images of brain sections from mice implanted with control-GFP-luciferase BT88 cells or CIC-GFP-luciferase BT88 cells stained with H&E or GFP. (C,C') Representative images of brain sections from mice implanted with control-GFP BT88 cells or DNETV5-GFP expressing BT88 cells stained with H&E or GFP. (D) Kaplan-Meier survival analysis of mice implanted with BT88 cell transfected with empty-GFP-luciferase or CIC-GFP-luciferase. (E) Kaplan-Meier survival analysis for BT88 cell transfected with empty-GFP or DNETV5-GFP.